Decoding m^{6}Am by simultaneous transcription-start mapping and methylation quantification

Jianheng Fox Liu[1], Ben R. Hawley[1, 2], Luke S. Nicholson[1], and Samie R. Jaffrey[1, *]

[1]Department of Pharmacology, Weill Cornell Medicine, Cornell University, New York, NY 10065, USA
[2]Present address: Engage Bio, San Carlos, CA, USA

*Correspondence should be addressed to S.R.J. (srj2003@med.cornell.edu)

ABSTRACT

N^6,2'-*O*-dimethyladenosine (m^{6}Am) is a modified nucleotide located at the first transcribed position in mRNA and snRNA that is essential for diverse physiological processes. m^{6}Am mapping methods assume each gene uses a single start nucleotide. However, gene transcription usually involves multiple start sites, generating numerous 5' isoforms. Thus, gene levels annotations cannot capture the diversity of m^{6}Am modification in the transcriptome. Here we describe CROWN-seq, which simultaneously identifies transcription-start nucleotides and quantifies m^{6}Am stoichiometry for each 5' isoform that initiates with adenosine. Using CROWN-seq, we map the m^{6}Am landscape in nine human cell lines. Our findings reveal that m^{6}Am is nearly always a high stoichiometry modification, with only a small subset of cellular mRNAs showing lower m^{6}Am stoichiometry. We find that m^{6}Am is associated with increased transcript expression and provide evidence that m^{6}Am may be linked to transcription initiation associated with specific promoter sequences and initiation mechanisms. These data suggest a potential new function for m^{6}Am in influencing transcription.

INTRODUCTION

m^{6}Am (*N*^{6},2'-*O*-dimethyladenosine) is the most common modified nucleotide in mRNA. m^{6}Am is found specifically at the first transcribed position of mRNAs, termed the transcription-start nucleotide (TSN), which reflects the transcription-start site (TSS) in DNA. During transcription, the TSN typically acquires a 2'-*O*-methyl modification[1,2], which is deposited by CMTR1 (Cap-specific mRNA nucleoside-2'-*O*-methyltransferase 1)[3]. In the case of mRNAs that use adenosine as the TSN, the initial 2'-*O*-methyladenosine (Am) can be further methylated on the *N*^{6} position of the adenine nucleobase to form m^{6}Am by PCIF1 (Phosphorylated CTD Interacting Factor 1)[4].

Studies using PCIF1 depletion (i.e., m^{6}Am depletion) have revealed that m^{6}Am has important roles in cell physiology. In normal cells, PCIF1 depletion does not appear to affect cell growth or viability[4]. However, in oxidative stress conditions, PCIF1 deficiency leads to impaired cell growth[4]. In cancer cells, PCIF1 depletion markedly enhances cell death during anti-PD1 therapy[5]. During viral infection, PCIF1 depletion results in increased HIV replication[6], impaired

SARS-Cov-2 infection[7], and increased VSV immunogenicity[8]. These studies indicate that m^6Am has important roles in diverse cellular contexts.

A major goal has been to identify and characterize the m^6Am- and Am-containing mRNAs. Initial chromatographic studies in the 1970s demonstrated that cellular mRNAs can exist in m^6Am and Am forms, with the Am form being more predominant[9]. To map m^6Am modified genes, several antibody-based methods were developed, including miCLIP[10], m^6Am-seq[11], m6ACE-seq[12], and m6Am-exo-seq[13]. These methods can identify m^6Am sites (miCLIP and m6ACE-seq), m^6Am peaks (m^6Am-seq), or m^6Am containing genes (m^6Am-exo-seq). Am genes were identified when m^6Am was not detected but the reported TSN in publicly available datasets was A. The remaining genes were annotated as Gm, Cm, or Um based on public TSS annotations.

However, despite these transcriptome-wide m^6Am maps, the effect of m^6Am on mRNA is unclear. By examining m^6Am genes, along with the change in mRNA stability and translation, small and inconsistent effects have been observed from different labs[4,13-15].

We considered the possibility that the difficulty in establishing m^6Am function may be due to flaws in the way that genes are designated as m^6Am genes. Previous m^6Am mapping studies treated m^6Am like other modified nucleotides, which are internal. In studies of internal nucleotides, such as m^6A, isoform diversity is generally not considered since these different isoforms rarely impact the detection of the nucleotide. In contrast, m^6Am is highly affected by isoform diversity since it is located at the 5' end. Most genes generate multiple transcript 5' isoforms that each use a different TSSs[16]. However, previous m^6Am mapping studies assumed that each gene has a single TSN, whose identity was based on existing gene annotations. Therefore, existing m^6Am maps that assign a specific start nucleotide to each gene cannot be accurate, since most genes produce a range of transcripts, with possibly multiple start nucleotides. For this reason, m^6Am mapping and functional studies of m^6Am need to be performed in a way that considers the 5' isoform diversity of most genes.

Another concern is that the existing m^6Am mapping studies designated each gene as either m^6Am or Am. However, it is possible that m^6Am levels can be variable, with only a fraction of transcripts containing m^6Am and the remainder containing Am. Stoichiometric maps of m^6Am can potentially reveal the degree to which a transcript would be influenced by m^6Am-dependent pathways.

Quantitative m^6Am mapping is especially important for small nuclear RNAs (snRNAs), which also contain m^6Am at their TSN. Initial biochemical characterization of snRNAs revealed that the first nucleotide was Am[17], but subsequent studies showed that nearly half of all snRNAs are initially methylated to m^6Am, and then demethylated by FTO to Am[10,12]. Thus, m^6Am is a transient intermediate in snRNA biogenesis. Notably, m^6Am levels can be highly regulated in snRNAs[10], however, current m^6Am mapping methods are unable to quantify changes in m^6Am stoichiometry.

87 To understand the transcriptome-wide distribution of m^6Am, we developed CROWN-seq
88 (**C**onversion **R**esistance detection **O**n **W**hole-transcriptomic transcription-start ***N***^{6},2'-*O*-
89 dimethyladenosine by **seq**uencing), an antibody-free quantitative m^6Am mapping method.
90 Using CROWN-seq, we define the overall repertoire of 5' isoforms for each gene, and the
91 specific isoforms that use m^6Am as the TSN across nine different cell lines. We find that
92 annotations of genes based on a single start nucleotide do not capture the diversity of 5'
93 transcript isoforms for most genes. Instead, m^6Am is more accurately assessed for each 5'
94 isoform separately. Nearly all A-initiated transcript isoforms have very high m^6Am stoichiometry,
95 and that transcripts containing Am as the TSN are relatively rare. Transcript isoforms that
96 contain m^6Am are more highly expressed, and loss of m^6Am due to depletion of PCIF1 leads to
97 reduced expression of transcript isoforms containing m^6Am. However, we find that this effect is
98 not due to decreased mRNA stability. Instead, the depletion of PCIF1 affects transcripts based
99 on upstream core promoter elements. Our data suggest that transcription mechanisms that
100 utilize specific core promoter sequences achieve high expression, which might be linked to a
101 transcription-promoting effect of m^6Am. Overall, our quantitative transcriptome-wide
102 transcription-start nucleotide m^6Am maps reveal a markedly distinct m^6Am profile than
103 previously measured, show that m^6Am is the predominant modified nucleotide relative to Am in
104 mRNA, and suggest roles of m^6Am in transcription.
105
106 **RESULTS**
107
108 **ReCappable-seq reveals high transcript isoform diversity at the 5' end**
109
110 In previous m^6Am mapping studies, genes were annotated to be m^6Am, Am, Gm, Cm, or Um
111 [4,10,13,14], based on the assumption that each gene has one major transcription-start nucleotide.
112 To determine how often genes are characterized by a single major TSS we used ReCappable-
113 seq[18], a method for quantitative measurement of transcription-start sites. ReCappable-seq is
114 similar to traditional TSS-seq methods which involve ligation of an oligonucleotide to the 5' end
115 of mRNAs[19], thus precisely marking the TSN. However, ReCappable-seq adds an enrichment
116 step for capped mRNA fragments to significantly reduce background signals from internal sites
117 that are derived from RNA cleavage. Thus, ReCappable-seq provides a highly sensitive and
118 precise mapping of TSNs at single-nucleotide resolution (**Note S1**, "The comparison of
119 transcription-start mapping methods").
120
121 By analyzing ReCappable-seq data in HEK293T cells, we found that protein-coding genes tend
122 to have multiple TSNs. Among the 9,199 genes analyzed, we identified 87,624 TSNs (see
123 **Methods**). On average, a gene uses 9.5±9 (mean and s.d., hereafter) TSNs (**Figure 1A**). Only
124 ~9% of genes contain a single TSN (**Figure 1A**). Thus, most genes cannot be characterized by
125 a single start nucleotide.
126
127 As an example, *SRSF1*, which was previously classified as a m^6Am gene, has ~37 different 5'
128 isoforms in HEK293T cells, of which ~41.5% do not use an A-TSN (**Figure 1B**). As another
129 example, *ADAR* was previously classified as a Gm gene, but ~71.0% of transcripts use A-TSNs

130 (**Figure 1C**). These observations are not artifacts of ReCappable-seq because similar results
131 were also found using other TSN mapping methods (**Figure S1A, S1B**).
132
133 Conceivably m^6Am genes produce multiple 5' isoforms, but the isoforms predominantly use A-
134 TSNs. If this were the case, then the gene could indeed be considered an m^6Am gene if all the
135 A-TSNs were methylated to m^6Am. We considered a gene to be predominantly composed of A-
136 TSNs if >80% of transcripts start with A. Using this criterion, we found that only ~24% of m^6Am
137 genes determined by miCLIP[14] are primarily composed of A-TSNs (**Figure 1D**). Similar
138 observations were also found in other m^6Am mapping methods[4,13] (**Figure S1C, D**).
139
140 Our ReCappable-seq analysis also suggested that previous m^6Am mapping methods may not
141 have detected the diversity of m^6Am in the transcriptome. ReCappable-seq identified many
142 more A-TSNs than the total number of previously mapped m^6Am sites. For example, in both
143 *SRSF1* and *ADAR*, many A-TSNs are seen using ReCappable-seq, however, m^6Am signals
144 were only found at a few of these A-TSNs by either miCLIP[14], m^6Am-seq[11], or m6ACE-seq[12]
145 (**Figure 1B, C**). This might suggest that only a few A-TSNs are m^6Am modified. However, it is
146 also possible that the antibody-based mapping methods do not have the resolution or sensitivity
147 to distinguish between m^6Am at different 5' isoforms. Notably, previous m^6Am mapping studies
148 exhibited very low overlap with each other. miCLIP[14], m^6Am-seq[11] and m6ACE-seq[12] together
149 identified 7,480 m^6Am sites in HEK293T cells (**Figure S1E** and **Table S1**). Among these sites,
150 only 1.1% (84) are found in all three methods and 9.7% (728) are found in at least two studies
151 (**Figure S1E** and **Table S1**). Taken together, these data demonstrate a variety of concerns
152 about existing m^6Am mapping studies.
153
154 **CROWN-seq integrates TSN mapping and m^6Am quantification**
155
156 To understand the distribution of m^6Am in the transcriptome, we sought to develop a method to
157 identify the entire repertoire of TSNs among all the 5' transcript isoforms for each gene. In this
158 way, we can identify the specific 5' isoforms for each gene that contain m^6Am. Additionally, we
159 wanted a quantitative method rather than the qualitative assessment provided by previous
160 antibody-based methods. Recently, chemical methods using sodium nitrite were developed for
161 m^6A analysis[20-22]. This method identifies m^6A by chemically deaminating ("converting")
162 unmethylated A's into inosines (I's), while leaving m^6A's intact. During sequencing, the A-to-I
163 conversions are readily detected because I's are reverse transcribed into G's. This approach
164 leads to precise and robust m^6A quantification[20]. Because of the chemical similarity between
165 m^6Am and Am, we explored the potential use of sodium nitrite conversion to map and quantify
166 m^6Am.
167
168 We first asked if Am is susceptible to deamination by sodium nitrite. To test this, we performed
169 sodium nitrite conversion on a m^7G-ppp-Am-initiated transcript (see **Methods**). We applied the
170 sodium nitrite conversion protocol used in GLORI, which includes glyoxal treatment to prevent
171 modification of guanosine residues[20]. After sodium nitrite treatment, the RNA was reverse
172 transcribed and sequenced. The conversion rate of Am was quantified by counting A or G
173 reads at the first nucleotide position. In this assay, Am was completely converted (**Figure S2A**),

174 indicating that sodium nitrite efficiently converts Am and thus can be used for m^6Am
175 quantification.
176
177 We considered the possibility that GLORI data[20] could be mined to measure m^6Am
178 stoichiometry at previously mapped m^6Am sites[14]. We noticed that many A's at these TSNs
179 were highly converted in GLORI (**Figure S2B**), suggesting prevalent Am. This is inconsistent
180 with mass spectrometry analysis of mRNA cap structures from us[1] and others[2,4], which has
181 suggested that m^6Am is very prevalent while Am is relatively rare in mRNA. A potential cause
182 of the high level of Am at TSNs predicted by GLORI could be the extensive RNA fragmentation
183 that occurs with sodium nitrite treatment. RNA fragments that have 5' ends that align to the
184 TSNs of overlapping transcript isoforms can confound the measurement of m^6Am stoichiometry
185 (**Figure S2C, S2D**). Thus, GLORI cannot distinguish between true TSNs and internal bases
186 that are found at the 5' end of RNA fragments. To overcome this limitation, we sought to
187 develop a method that selectively analyzes A-TSNs and thereby removes the confounding
188 effect of overlapping transcripts.
189
190 We developed CROWN-seq, which selectively analyzes TSNs throughout the transcriptome
191 (**Figure 2A**). In this method, Am residues in mRNA are converted to Im using sodium nitrite.
192 Next, we specifically isolate the 5' ends of mRNA by replacing the m^7G cap with a desthiobiotin
193 affinity tag using a decapping-and-recapping strategy[18]. By enriching the m^7G-proximal
194 sequence, we can simultaneously sequence the TSN of all transcripts, including both m^6Am and
195 non-m^6Am TSNs. This is conceptually different from existing m^6Am mapping methods which
196 only examine the m^6Am transcripts. For A-TSNs, m^6Am stoichiometry can be quantified by
197 counting the number of A reads (reflecting m^6Am) or G reads (reflecting Am). In this way, we
198 not only obtain TSN locations but also m^6Am stoichiometry in the same RNA molecule.
199
200 To increase the accuracy of m^6Am quantification, we made several optimizations to the
201 ReCappable-seq protocol to markedly increase the read depth of TSNs. These include steps
202 for on-bead adapter ligation and the introduction of unique molecular identifiers (UMIs) in the
203 library preparation (see **Methods**).
204
205 **Benchmarking CROWN-seq using m^6Am-modified standards**
206
207 To test TSN enrichment in CROWN-seq, we used a m^7G-ppp-m^6Am standard spiked into
208 cellular mRNA. Among three replicates, we observed that ~93% of the reads mapped to the
209 TSN (**Figure 2B**), confirming the enrichment of TSN. To further assess the enrichment of
210 TSNs, we performed GLORI on the same sample. However, in GLORI only a few reads map to
211 the TSN (**Figure S2C**). Thus, the decapping-and-recapping approach markedly enriches for
212 TSNs.
213
214 We next wanted to determine the quantitative accuracy of CROWN-seq. To test this, we
215 performed CROWN-seq on a mixture of RNA standards with predefined ratios of m^6Am and Am
216 (see **Methods** and **Table S2**). We found a highly linear correlation between the expected m^6Am
217 levels and the observed non-conversion rates measured by CROWN-seq across three

218 replicates (Pearson's r = 0.992, **Figure 2C**). Taken together, CROWN-seq achieves both
219 precise TSS mapping and m^6Am quantification in m^6Am standards.
220
221 **CROWN-seq markedly expands the number of mapped m^6Am sites**
222
223 To assess the ability of CROWN-seq to map and quantify m^6Am throughout the transcriptome,
224 we performed CROWN-seq on poly(A)-selected RNA from HEK293T. In total, we identified
225 219,195 high-confidence TSNs, of which 92,278 were A-TSNs **(Note S2**, "Selection of m^6Am
226 identification cutoffs"). These TSNs were highly reproducible across biological and technical
227 replicates (**Figure S2E**). Among the A-TSNs, 89,898 were from protein-coding genes, and 219
228 were from snRNA or snoRNA. Notably, among the mRNA A-TSNs, nearly all had high non-
229 conversion rates (**Figure S2F**), indicating that nearly all A-TSNs contain high stoichiometry
230 m^6Am.
231
232 In contrast to previous m^6Am mapping methods, CROWN-Seq reveals the diversity of TSNs
233 among all the transcript isoforms for each gene. For example, in the case of *SRSF1*, m^6Am is
234 readily visible along with multiple other TSNs comprising Gm, Cm, or Um (**Figure 2D**).
235 CROWN-seq also shows that A-TSNs can have intermediate m^6Am stoichiometry. For example,
236 *JUN* expresses a 5' transcript isoform with an A-TSN, of which ~75% of transcript copies are
237 m^6Am modified (**Figure 2E**). Overall, CROWN-seq provides a comprehensive assessment of all
238 TSNs in a gene and reveals the fraction of each A-TSN that is m^6Am.
239
240 To confirm the accuracy of the mapped m^6Am TSNs, we examined the 7,480 m^6Am sites
241 reported by miCLIP[14], m^6Am-seq[11], or m6ACE-seq[12]. Among these sites, the vast majority
242 (~82.8%, 6,196 of 7,480) were also found among the high-confidence A-TSNs in CROWN-seq
243 (**Figure 2F**). For the remaining 1,284 sites, 811 are also found in CROWN-seq, but in lower
244 sequencing depth; 319 were located far away (>100 nt) from any known TSSs and thus may be
245 artifacts. Thus, CROWN-seq is highly reliable in detecting known m^6Am sites. The low
246 consistency between previous m^6Am mapping studies likely reflects incomplete m^6Am mapping
247 in previous methods.
248
249 CROWN-seq clearly identified vastly more A-TSNs than all the other m^6Am mapping methods
250 combined (12.3-fold, 92,278 vs. 7,480). Notably, only ~12.2% of the newly found A-TSNs in
251 CROWN-seq are annotated in Gencode v45 (**Figure 2G, S2G**), which primarily relies on CAGE
252 data (see gene annotation guidelines by HAVANA[23]). Notably, the newly identified TSNs with
253 high coverage tend to overlap with or locate proximally to known TSSs, while the ones with low
254 coverage tend to locate further to the known TSSs (**Figure S2G**). The newly identified A-TSNs
255 could be artifacts or could be actual TSNs that were undetected by previous TSS-mapping
256 studies. We suspect that these are true A-TSNs for two reasons: First, as part of the mapping
257 criteria, a minimum of 20 independent reads across all replicates was required for TSN
258 identification. Second, if these sites were RNA fragments, they would not contain m^6Am.
259 However, these A-TSNs show high stoichiometry of m^6Am (i.e., non-conversion) in CROWN-
260 seq (**Figure 2H, S2F**) which is lost in *PCIF1* knockout cells (**Figure 2H**), except for some
261 outliers such as TSNs of *S100A6*, *IFI27*, and *ALDH1A1* (see **Table S3**). Thus, the marked

262 increase in the number of m^6Am sites revealed by CROWN-seq reflects the preferential
263 enrichment for mRNA 5' ends, which leads to high sensitivity and read depth at TSNs
264 transcriptome-wide.
265
266 In contrast to m^6Am sites identified in CROWN-seq, m^6Am that were identified in previous m^6Am
267 mapping methods tended to derive from high abundance transcripts or high abundance TSNs
268 (**Figure 2I**). Because of the high read depth at TSNs, CROWN-seq enables the detection of
269 m^6Am at more m^6Am sites than previous methods (**Figure 2J**, **Figure S2H**). Although we used
270 a 20-read cutoff for mapping m^6Am, m^6Am sites identified with fewer reads are also likely to
271 represent true TSNs. These m^6Am TSNs typically show high non-conversion (e.g., 2 or 3 reads
272 among a total of 3 reads) in HEK293T cells but zero non-conversions in *PCIF1* knockout cells
273 (**Figure S2I**). The PCIF1 dependence of these sites is consistent with a true m^6Am TSN and
274 further highlights the sensitivity of CROWN-seq for mapping m^6Am at TSNs.
275
276 **CROWN-seq reveals consistently high m^6Am stoichiometry in mRNA across diverse**
277 **human cell lines**
278
279 Although our data showed that m^6Am in mRNA generally exhibits very high stoichiometry
280 (**Figure S2F**), we considered the possibility that these results were unique to HEK293T cells.
281 Several studies have shown that PCIF1 expression can vary considerably in different cell
282 lines[5,24], which may indicate that m^6Am stoichiometry is dependent on the cell line. We therefore
283 wanted to determine the m^6Am landscape across cell lines with varying levels of PCIF1.
284
285 We selected several cell lines for this analysis. First, we chose HEK293T, A549, HepG2, and
286 K562 cells, which have also been characterized using multiple orthogonal datasets[25]. Second,
287 we selected colorectal cancer cells (i.e., HT-29 and HCT-116), since PCIF1 depletion in these
288 cells affects their migration and sensitivity to immunotherapy[5]. These colorectal cancer cells
289 have high PCIF1 expression based on western blotting and RT-qPCR, while the non-cancerous
290 colon cell line CCD841 CoN has very low PCIF1 expression[5]. Third, we selected cells with very
291 low CTBP2 expression, a proposed coactivator of PCIF1[24]. These cells, which include Jurkat
292 E6.1 and Huh-7, as well as the previously mentioned K562 and HepG2 cells, would be expected
293 to have low m^6Am levels based on their low CTBP2 expression[24] (**Figure S3A**).
294
295 For each cell line, we performed CROWN-seq using two to four replicates. In total, we obtained
296 514 million aligned reads (**Table S3**). In each cell line, 14,650 to 58,768 mRNA A-TSNs with at
297 least 50 reads were analyzed (**Table S3**). The 50-read threshold provides highly consistent
298 quantification of m^6Am stoichiometry between replicates (**Figure S3B** and **Note S2**).
299
300 Quantification of m^6Am across all TSNs showed that mRNA m^6Am stoichiometry is generally
301 high. For most of the cells, the average m^6Am stoichiometry is 0.895±0.03 (**Figure 3A**),
302 indicating high overall mRNA m^6Am levels. Some cell lines, for example, Jurkat E6.1, HT-29,
303 and Huh-7 cells show very high and less variable m^6Am levels (0.933±0.1, 0.924±0.1, and
304 0.916±0.1, respectively); while other cell lines such as CCD841 CoN, HCT-116, and K-562 have
305 relatively low and more variable m^6Am levels (0.825±0.2, 0.877±0.1, and 0.891±0.1,

306 respectively). It should be noted that in all cell lines, the m^6Am stoichiometry is still high
307 compared with other mRNA modifications[20].
308
309 We considered the possibility that the high m^6Am stoichiometry might be caused by RNA
310 structure that blocks access to sodium nitrite leading to non-conversion. However, essentially
311 complete conversion was seen in *PCIF1* knockout HEK293T cells, which makes it likely that
312 m^6Am is the cause of non-conversions. Also, we found that A-TSNs completely converted in 5'
313 ends predicted to be highly structured, suggesting that RNA structure does not impair
314 conversion in CROWN-seq (**Figure S3C**).
315
316 The differences in m^6Am stoichiometry are related to PCIF1 expression (**Figure 3B, S3D**). For
317 example, CCD841 CoN cells, which have very low PCIF1 expression based on our
318 measurements (**Figure 3B, S3D**) and previous measurements[5], exhibit the lowest median
319 m^6Am stoichiometry at ~0.878. However, even this stoichiometry is still relatively high. Thus,
320 m^6Am levels are affected by PCIF1 expression, but m^6Am can be considered as a high
321 stoichiometry modification across all tested cell lines. On the other hand, the proposed PCIF1
322 coactivator CTBP2, exhibited a weak correlation to mRNA m^6Am (**Figure 3C**).
323
324 **Several mRNAs show low m^6Am stoichiometry**
325
326 Although most A-TSNs in mRNA exhibit high m^6Am stoichiometry, some exhibit stoichiometry
327 below 0.8, and even below 0.5 (**Figure 3A** and **Table S3**). To identify A-TSNs with low m^6Am,
328 we examined each A-TSN and calculated its average stoichiometry across all cell lines (**Figure**
329 **3D**). For each A-TSN we also assessed its variability by calculating the range of m^6Am levels
330 measured across cell lines (**Figure 3D**). This analysis demonstrates that a significant subset of
331 A-TSNs have low stoichiometry, with some showing variability depending on the cell type. For
332 example, *JUN* contains a lowly methylated A-TSN, as shown above in HEK293T cells (**Figure**
333 **2E**), and also exhibits low stoichiometry in many other cell lines (**Figure 3E**). In addition, *ENO1*,
334 *MYC*, and *ACTB* also show low m^6Am stoichiometry in some of their A-TSNs (**Figure 3E**).
335
336 We next used Gene Ontology (GO) analysis to determine if the low m^6Am A-TSNs are
337 associated with specific cellular functions. The GO analysis of Cellular Component categories
338 showed a marked enrichment of genes linked to cellular respiration, ribosomal subunits,
339 spliceosome, and nucleosome (which are mostly histone genes) (**Figure 3F**, **Table S4**). Similar
340 results were found in the Biological Processes GO analysis (**Table S4**). In addition to these
341 genes, we also noticed HOX genes contain lowly methylated A-TSNs (**Figure S3E**).
342
343 Among all different gene categories, histone genes exhibited the lowest overall m^6Am
344 stoichiometry (**Figure 3G**). Notably, histone genes have unique mechanisms of gene
345 expression. Many histone genes are located in gene clusters (i.e., clusters 6p22.1-2 and
346 1q21.1-2) and transcribed in histone locus bodies[26]. These clustered histone genes tend to
347 contain upstream TATA-box and downstream T-rich sequences (**Figure S3F**). In contrast, non-
348 clustered histone genes tend to have high m^6Am stoichiometry (**Figure 3G**) and show different

349 promoter sequence contexts (**Figure S3F**). This data suggests that transcription mechanisms
350 might be important for determining m^6Am stoichiometry.
351
352 **m^6Am stoichiometry is linked to the sequence of core promoter**
353
354 The differential methylation in histone genes based on their transcription mechanisms raises the
355 possibility that transcription initiation mechanisms might affect m^6Am stoichiometry. Because
356 m^6Am is the first nucleotide in mRNA, its deposition may be highly influenced by early
357 transcription events. Notably, PCIF1 binds to RNA polymerase II[27] and is enriched in promoter
358 regions[28], which may be important for methylation of the 5' end of mRNAs. We therefore
359 considered the possibility that different transcription mechanisms may be linked to different
360 levels of m^6Am.
361
362 As a first test, we examined whether nucleotide preferences upstream (which would reflect
363 sequences involved in transcription initiation) or downstream of the A-TSN are linked to m^6Am
364 stoichiometry. We binned A-TSNs based on the m^6Am stoichiometry and examined nucleotide
365 preferences at each position. Using this approach, we found that the nucleotides upstream of
366 the A-TSN were markedly different for A-TSNs with low vs. high m^6Am stoichiometry (**Figure**
367 **S4A**). For example, at positions -4 and -1, there was a clear positive correlation between the
368 use of C and m^6Am stoichiometry (**Figure 4A**). The correlation of these nucleotide positions
369 that lie in the promoter region to m^6Am stoichiometry suggests that transcriptional mechanisms
370 might influence m^6Am stoichiometry.
371
372 We also observed strong nucleotide preferences at positions downstream of the A-TSN. These
373 include nucleotide preferences at +2 (**Figure 4A**). These could reflect sequence preferences
374 for PCIF1; however, this position is also part of transcription-initiation motifs (see below), and
375 thus the contribution of transcription mechanisms and direct sequence preferences of PCIF1 are
376 difficult to deconvolve.
377
378 To more directly determine specific transcription mechanisms linked to m^6Am, we examined
379 how specific sequence motifs around A-TSNs correlate with m^6Am stoichiometry. We found
380 markedly different sequence motifs surrounding highly methylated A-TSNs compared to lowly
381 methylated A-TSNs (**Figure 4B**). A-TSNs with the highest m^6Am stoichiometry (top 5th-
382 percentile, 0.991 average stoichiometry) are enriched in an $SSCA_{+1}GC$ (S=C/G) motif, which is
383 similar but distinct from the well-known $BBCA_{+1}BW$ (B=C/G/T, W=A/T) transcription initiator
384 motif[29], largely because of the C at the +3 position (**Figure 4B**). In contrast, the A-TSNs with
385 the lowest m^6Am stoichiometry (bottom 5th-percentile, 0.435 average stoichiometry) were
386 enriched in an unconventional $VA_{+1}RR$ (V=A/C/G, R=A/G) motif (**Figure 4B**).
387
388 We next classified each A-TSN based on whether they use the $SSCA_{+1}GC$ or $VA_{+1}RR$ motifs, or
389 if they contain the conventional $BBCA_{+1}BW$ and BA_{+1} Inr-like motifs (**Figure S4B**). This plot
390 shows that $BBCA_{+1}BW$ and BA_{+1} motifs exhibit intermediate m^6Am stoichiometry (**Figure 4C**).
391 Overall, these data indicate that m^6Am stoichiometry is strongly related to the TSS motif in the
392 core promoter, which implies that m^6Am formation is linked to the transcription initiation process.

393
394 Because transcription initiation is also affected by other elements in the core promoter[29], we
395 also asked whether these transcription-related elements, such as TATA-box and transcription
396 factor-binding sites, are associated with higher or lower m^6Am stoichiometry. We first analyzed
397 the relationship between m^6Am and elements including the TATA-box, BREu, BREd, and
398 DCE[29]. In this analysis, A-TSNs from promoters containing TATA-box exhibited lower m^6Am
399 stoichiometry, especially those of histone genes (**Figure 4D**). On the other hand, other
400 elements, such as BREu and BREd, which are motifs for recruitment of TFIIB[29], and DCE,
401 which binds by TAF1[29], showed little correlation with m^6Am stoichiometry (**Figure S4C**). Thus,
402 the presence of the TATA box exhibited the strongest effect and predicted lower m^6Am
403 stoichiometry.
404
405 We next analyzed the relationship between m^6Am and transcription factor-binding sites (TFBS).
406 To test this, we screened A-TSNs for the presence of 401 transcription-factor binding sites and
407 examined the relationship between the binding sites and m^6Am stoichiometry (see **Methods**).
408 Several TFBSs, such as those for NANOG and FOXJ3, exhibited a slight negative correlation to
409 m^6Am (**Figure S4D**); while other TFBS, such as SP2 and KLF4, exhibited a slight positive
410 correlation to m^6Am (**Figure S4E**). Overall, no specific TFBS exhibited a strong effect on m^6Am
411 stoichiometry (**Figure S4F**).
412
413 Taken together, our data show a linkage between transcriptional mechanisms and m^6Am
414 stoichiometry.
415
416 **m^6Am does not substantially influence mRNA stability or translation**
417
418 Previous studies sought to determine the effect of m^6Am on mRNA stability and translation
419 based on gene-level annotations of the starting nucleotide[4,14,15,30]. However, the gene level
420 annotations do not take into account the potential for many transcription-start nucleotides
421 (**Figure S5**). Rather than using a binary metric of m^6Am or non-m^6Am, we developed a metric
422 that reports the fraction of all TSNs for each gene that contain m^6Am. This "m^6Am gene index"
423 is the ratio of m^6Am TSNs over all TSNs, as measured by CROWN-seq, for each gene. Using
424 the m^6Am gene index, we reanalyzed the previously published translation efficiency[4,14] and RNA
425 stability[14] data in HEK293T cells. We found that genes with low or high m^6Am gene index do
426 not show differences in translation (**Figure S6A, S6B**) or RNA stability (**Figure S6C**) in *PCIF1*
427 knockout cells compared to wild-type.
428
429 **m^6Am is involved in efficient transcription of A-initiated transcripts**
430
431 We next wanted to examine other potential functions of m^6Am. Although we found no clear
432 effect of m^6Am on mRNA stability, we asked if m^6Am influences transcript expression levels. To
433 test this, we quantified the abundance of each A-TSN isoform in HEK293T and A549 cells. For
434 these experiments, we added a mixture of pre-capped ERCC spike-ins (see **Methods**) to the
435 RNA samples before performing TSN expression quantification by ReCappable-seq. This

436 ERCC spike-in mixture calibrates sequencing results and increases TSN expression
437 quantification accuracy (see **Methods**).
438
439 In this analysis, we binned A-TSNs into percentiles based on their m^6Am stoichiometry. Here we
440 could see that transcripts with the highest levels of m^6Am also exhibited the highest overall
441 expression levels (**Figure 5A**, **S6D**, and **Table S5**). This suggests that m^6Am is associated with
442 higher transcript expression.
443
444 To determine if m^6Am causes the increased expression of A-TSN transcripts, we measured the
445 expression change for each A-TSN in wild-type and *PCIF1* knockout HEK293T and A549 cells
446 (**Table S5**). We found that A-TSNs with higher m^6Am stoichiometry exhibit significantly reduced
447 expression in *PCIF1* knockout, while A-TSNs with the lowest m^6Am stoichiometry were almost
448 unchanged (**Figure 5B, S6E**). In contrast, G-TSNs were slightly increased in *PCIF1* knockout
449 cells (**Figure 5C, S6F**). These data suggest that m^6Am promotes the expression of A-TSN
450 transcripts.
451
452 We were surprised that PCIF1 depletion leads to a selective decrease in the expression of A-
453 TSN transcripts in the highest percentile bin but had little to no effect in the other bins. Each bin
454 has very high m^6Am stoichiometry (~0.77 in the lowest bin and ~0.98 in the highest bin in
455 HEK293T) (**Figure 5B, S6E**). Thus, if m^6Am is a stabilizing mark, we should see reduced
456 expression in all bins. We therefore considered other possibilities that might explain why PCIF1
457 depletion affects transcript levels in some bins but not others.
458
459 An important difference between A-TSN in different bins is that they tend to use different TSS
460 motifs (see **Figure 4C**). We therefore asked if the effect of m^6Am depletion is linked to the TSS
461 motifs. For this analysis, we classified A-TSNs based on the presence of $SSCA_{+1}GC$, $VA_{+1}RR$,
462 or other TSS motifs (i.e., $BBCA_{+1}GC$ and BA_{+1}). Here we found that the identity of the TSS motif
463 was highly associated with the degree of transcript reduction in *PCIF1* knockout cells (**Figure**
464 **5D, S6G**). Notably, transcripts that use the $SSCA_{+1}GC$ motif showed the largest drop in
465 expression. In contrast, A-TSNs that use the $VA_{+1}RR$ TSS motif showed almost no change in
466 expression in *PCIF1* knockout cells (**Figure 5D, S6G**).
467
468 Taken together, these data suggest that the effect of m^6Am is not related to mRNA stability but
469 instead is related to transcription. Our data suggest that certain transcription initiation
470 complexes, such as those that use the $SSCA_{+1}GC$ motif, rely on m^6Am for efficient expression.
471 However, other TSS motifs do not rely as strongly on m^6Am to achieve efficient expression.
472 These data suggest that m^6Am may have important roles in the transcription processes.
473
474 **CROWN-seq reveals diverse m^6Am stoichiometry in snRNA and snoRNA**
475
476 In addition to mRNAs, m^6Am is also found on snRNAs and snoRNA[10,12]. However, the
477 stoichiometry and dynamics of m^6Am in these RNAs are unknown. Using CROWN-seq we
478 quantified m^6Am stoichiometry in several snRNAs, including U1, U2, U4, U4ATAC, U5, U7, U11,
479 and U12. These snRNAs are transcribed by RNA polymerase II[31], are capped, and use A-

480 TSNs[10]. Among these snRNAs, we identified 51 m^6Am sites, of which 29 were unannotated 5'
481 variants located close to the annotated TSNs (**Table S6**).
482
483 Compared with mRNA, m^6Am in snRNA exhibited a very different distribution of stoichiometry
484 (**Figure S2F**). First, snRNA m^6Am sites exhibited generally low m^6Am stoichiometry, typically
485 below 0.3. Second, m^6Am stoichiometry between different snRNA genes was much more
486 variable than in mRNA (**Figure 6A**). Third, some snRNA genes show highly variable
487 stoichiometry in different cell lines.
488
489 For example, among U1 snRNA genes, *U1.22* exhibited relatively high m^6Am levels (~0.47-
490 0.80) in all cell lines, while *RNU1-3* and *RNU1-4* show relatively low m^6Am levels (~0.09-0.45,
491 **Figure 6A** and **Table S6**). U5 snRNAs have the highest variability m^6Am stoichiometry
492 between cell types (**Figure 6A**). The U5 snRNA isoform *RNU5E-1* varies 31.6-fold in the m^6Am
493 level between HEK293T (0.0185) and Jurkat E6.1 cells (0.586). In contrast, m^6Am in U2 and
494 U7 snRNA are generally high (at 0.35-0.76 and 0.48-0.89, respectively) and not variable
495 between cell lines (**Figure 6A**).
496
497 In addition to snRNA, we also examined 17 A-TSNs in C/D box snoRNA including U3, U8, and
498 U13. These snoRNAs are involved in rRNA 2'-*O*-methylation during pre-rRNA processing[32].
499 m^6Am stoichiometry in snoRNA is highly related to snoRNA species and snoRNA isoform. For
500 example, among different U3 snoRNA isoforms, A-TSNs of *U3.18* have much higher m^6Am
501 stoichiometry than others (e.g., *SNORD3A*) (**Figure 6B**). These data indicate that snoRNA also
502 has highly variable m^6Am stoichiometry.
503
504 **FTO specifically controls m^6Am stoichiometry in snRNA and snoRNA**
505
506 We next sought to understand why m^6Am stoichiometry is low in snRNA and snoRNA. We
507 considered the possibility that the overall m^6Am stoichiometry in snRNA is correlated with PCIF1
508 expression, as we saw with mRNA (**Figure 3B**). However, we found a poor correlation of
509 overall m^6Am stoichiometry in snRNA with PCIF1 expression (Pearson's r = 0.204, P-
510 value=0.597, **Figure 6C**).
511
512 We next considered FTO, a highly efficient demethylase for m^6Am in snRNA[10,12]. In contrast to
513 PCIF1, FTO expression exhibited a strong negative correlation with snRNA methylation levels
514 (Pearson's r = -0.773, P-value=0.014, **Figure 6D**). Notably, HEK293T cells, which were tested
515 in our previous study[10], exhibited the highest FTO expression and the lowest snRNA m^6Am
516 stoichiometry (**Figure 6D**). Some other cell lines, such as Huh-7, have lower FTO expression
517 and thus have relatively higher m^6Am stoichiometry in snRNAs (**Figure 6D**).
518
519 We next wanted to determine how FTO affects m^6Am stoichiometry in snRNAs. Using CROWN-
520 seq on *FTO* knockout HEK293T cells, we observed prominent m^6Am level increases in nearly
521 all snRNA and snoRNA (**Figure 6E**). Most of the snRNA isoforms exhibited an overall increase
522 in m^6Am stoichiometry by ~0.2 upon *FTO* knockout. However, a notable subset of snRNAs
523 were not affected by FTO depletion. For example, the *RNVU1-8* isoform has little change in

524 m^6Am stoichiometry. *RNVU1-8* has an unusually high m^6Am stoichiometry at ~0.47 compared
525 to other U1 snRNA isoforms in wild-type cells (**Figure 6E**).
526
527 Notably, FTO depletion does not increase m^6Am levels in snRNA and snoRNA to the levels
528 seen in mRNA (i.e. >0.9 stoichiometry). This suggests that the low m^6Am levels in snRNA and
529 snoRNA are not solely due to FTO-mediated demethylation. Instead, these snRNAs are likely
530 to be inefficiently methylated by PCIF1 and are then demethylated by FTO in order to achieve
531 their overall low m^6Am stoichiometry.
532
533 We also found FTO demethylates m^6Am in snRNA pseudogenes. Overall, we mapped 69 A-
534 TSNs in annotated snRNA/snoRNA pseudogenes. These pseudogenes exhibited increased
535 methylation upon *FTO* knockout (**Figure 6F** and **Table S6**). We also identified 202
536 snRNA/snoRNA pseudogene-like transcripts (see **Table S6**). These transcripts exhibited very
537 high similarity to the annotated snRNA/snoRNA pseudogenes, and therefore likely reflect
538 previously unannotated pseudogenes (see **Methods**). Upon *FTO* knockout, A-TSNs in these
539 unannotated pseudogenes also exhibited increased m^6Am levels (**Figure 6F**).
540
541 **FTO has minimal effects on m^6Am and m^6A at 5' ends of mRNA**
542
543 We next asked whether FTO levels affect m^6Am levels in mRNA. To address this question, we
544 compared FTO RNA expression and median mRNA m^6Am stoichiometry in all nine cell lines.
545 This analysis shows a weak negative correlation between FTO expression and mRNA m^6Am
546 (Pearson's r = -0.239, P-value=0.535, **Figure S7A**).
547
548 To further assess whether FTO affects m^6Am levels in mRNA, we quantified m^6Am level
549 changes in mRNA in wild-type and *FTO* knockout HEK293T cells. Overall, we observed a very
550 small increase in mRNA m^6Am with only a few m^6Am sites having notably increased methylation
551 level upon *FTO* knockout (**Figure S7B**). Thus, only select m^6Am sites in mRNA are efficiently
552 demethylated by FTO.
553
554 Although CROWN-seq focuses on m^6Am measurements, the reads in CROWN-seq can contain
555 internal m^6A sites if they are close to the TSN. m^6A sites are readily detected because they do
556 not undergo conversion with sodium nitrite. We therefore examined the stoichiometry of these
557 5'-proximal m^6A sites in *FTO* knockout HEK293T cells. We identified internal m^6A sites that
558 were mapped with at least 50 reads in both wild-type and *FTO* knockout cells and had a non-
559 conversion rate of ≥0.2 in either genotype. In total, we identified 235 high-confidence m^6A sites
560 which were found by both CROWN-seq and GLORI[20](**Table S6**). These m^6A sites exhibited the
561 expected DRm^6ACU motif (**Figure S7C**). However, these sites only showed small changes in
562 non-conversion rates (P-value=0.00037, paired t-test) (**Figure S7D** and **Figure S7E**). It should
563 be noted that our conclusion about the effect of FTO on internal m^6A is restricted to specific m^6A
564 sites around 5' ends since most internal m^6A sites are not found in the 5' fragments examined in
565 CROWN-seq.
566

567 Taken together, FTO has a strong preference for demethylating m^6Am in snRNA, snoRNA, and
568 their pseudogenes, compared to mRNA. FTO is a major determinant of the overall m^6Am levels
569 of these transcripts in different cell lines.
570
571 **DISCUSSION**
572
573 Functional studies of m^6Am require highly accurate transcriptome-wide maps. However, m^6Am
574 mapping studies have relied on the assumption that each gene can be considered to have a
575 single start nucleotide. To overcome this, we developed CROWN-seq, which maps the TSNs
576 for all 5' transcript isoforms, and measures the exact stoichiometry of m^6Am at all A-TSNs.
577 CROWN-seq reveals a markedly distinct distribution of m^6Am than previously recognized,
578 largely due to inaccuracies in previous maps, and the problem with assigning each gene to a
579 single start nucleotide. In addition, the quantitative measurements of m^6Am in CROWN-seq
580 show that the earlier idea that many mRNAs contain transcription-start nucleotide Am is largely
581 incorrect since nearly all A-TSNs exhibit high stoichiometry m^6Am. Overall, this study
582 establishes the first quantitative, transcript isoform-specific m^6Am map in mammalian cells. The
583 m^6Am maps reveal that m^6Am is associated with increased transcript abundance, with functions
584 of m^6Am more correlated with transcription initiation than stability.
585
586 By selectively capturing and examining only 5' ends, CROWN-seq achieves exceptional read
587 depth at the TSN, enabling highly accurate identification and quantification of m^6Am. Notably,
588 CROWN-seq is an antibody-free method and thus avoids the problem of immunoprecipitation of
589 both m^6Am- and m^6A-containing fragments. This dual-specificity of antibodies creates
590 ambiguities in m^6Am mapping. Additionally, antibody binding cannot provide quantitative
591 measurements of m^6Am. In contrast, CROWN-seq uses a sodium nitrite-based chemical
592 method for m^6Am identification, which we show fully converts Am to Im, but leaves m^6Am intact.
593 Thus, the fraction of A-TSNs that contain m^6Am or Am can be readily determined by
594 sequencing, where all Am nucleotides are read as G. The exceptional read depth of CROWN-
595 seq enables quantification of m^6Am at single-nucleotide resolution, resulting in vastly more
596 m^6Am sites than all previous m^6Am mapping methods combined. Although CROWN-seq
597 involves many chemical and enzymatic steps, m^6Am quantification by CROWN-seq is very
598 accurate and robust, which was examined by m^6Am standards, consistency across different
599 replicates, and *PCIF1* knockout data. Notably, chemical conversion-based methods tend to
600 have artifacts in regions with stable RNA secondary structures[33,34], where the nucleotides
601 cannot efficiently interact with the chemical reagent. However, we found that CROWN-seq is
602 very reliable even for highly structured 5' ends (**Figure S3C**), which might be due to the high
603 accessibility of the TSN, the high stringency of the conversion steps[20], or RNA denaturation due
604 to glyoxal[35].
605
606 It is worth mentioning that there is no golden standard for transcription-start nucleotide (site)
607 mapping accuracy estimation. For CROWN-seq, we first tested the mapping accuracy by *in*
608 *vitro* transcribed RNA oligos, which shows that ~93% of the 5' ends can be mapped correctly.
609 However, in practice, *in vitro* transcription might initiate at non-specific TSSs, resulting in 5' ends
610 not overlapping with the desired TSSs[36,37]. Thus, the mapping accuracy can be underestimated

611 in this assay. Since mRNA A-TSNs in the cells are known to be highly methylated by PCIF1[1,4],
612 we considered that the presence or absence of m^6Am at mapped A-TSNs can be used to
613 assess the accuracy of TSN identification. True A-TSNs should have m^6Am. In CROWN-seq
614 essentially all previously annotated A-TSNs and newly found A-TSNs exhibited high non-
615 conversion rates. These A-TSNs were well converted upon *PCIF1* knockout. This indicates
616 very high TSN mapping accuracy, even at the many previously unannotated TSNs described
617 here. These previously unannotated TSNs were likely missed because traditional transcription-
618 start mapping methods and pipelines lack the sensitivity to discover them. These unannotated
619 TSNs might have specific molecular functions. Future studies might focus on the biology of
620 these unannotated TSNs, for example, whether these unannotated TSNs, compared to major
621 TSNs, are associated with different mRNA processing events, such as alternative splicing.
622
623 We performed CROWN-seq in nine different cell types with the goal of understanding common
624 principles that guide m^6Am formation in mRNA. In all cell types, m^6Am was a very high
625 stoichiometry modification, with some exceptions. We found a correlation between PCIF1
626 expression and m^6Am stoichiometry, but even cells with very low PCIF1 expression exhibited
627 high m^6Am stoichiometry. The CROWN-seq data is highly consistent with recent mass
628 spectrometry analysis of mRNA caps by us[1] and others[2,4]. These mass spectrometry studies
629 purified the entire cap structure comprising the m^7G, the triphosphate linker, and the first
630 nucleotide. In these studies, m^7G-ppp-m^6Am was highly prevalent while m^7G-ppp-Am
631 abundance was typically 1/10 as m^7G-ppp-m^6Am in nearly all cell lines[1,2]. This mass
632 spectrometry data was the first suggestion that transcription-start nucleotide Am was not a
633 prevalent modification in mRNA, as had been suggested by early chromatography studies[9]. We
634 suspect that the high levels of Am seen in these early analyses of mRNA can be explained by
635 contaminating snRNA or rRNA fragments, which are highly difficult to remove, even with
636 multiple rounds of poly(A) purification[38]. It remains possible that there are cell types or cellular
637 contexts that remain to be discovered with low m^6Am (i.e., high Am) levels. However, it is clear
638 that high m^6Am stoichiometry is a general feature of most or all cell types in this study.
639
640 The initial m^6Am maps relied on published TSN annotations. In the first m^6Am map, annotations
641 were based on FANTOM5[16], which primarily uses CAGE datasets to define the start nucleotide.
642 However, these annotations selected a single start nucleotide even if multiple TSS signals from
643 CAGE peaks were detected for a gene[4,14]. It should be noted that some genes may primarily
644 use m^6Am for all 5' transcript isoforms. These genes would therefore have a high m^6Am gene
645 index. Genes with a high m^6Am gene index are likely to be preferentially affected by PCIF1
646 depletion or pathways that affect m^6Am.
647
648 Based on the small range of m^6Am stoichiometry in A-initiated mRNAs, it is unlikely that the
649 variability in stoichiometry has functional significance for most mRNAs. Instead, our data
650 suggest that mRNAs initiate with either Gm, Cm, Um, or Am, where Am is highly m^6Am
651 modified. mRNAs that initiate with m^6Am may have shared regulatory mechanisms that
652 distinguish them from mRNAs that initiate with Gm, Cm, and Um. Additionally, genes that
653 primarily initiate with m^6Am, either because they have only one major transcription-start site, or
654 because all their transcription-start nucleotides are A, would be highly influenced by m^6Am-

655 dependent regulatory mechanisms. Currently, cellular pathways that target m^6Am-initiated
656 mRNAs are not well known.
657
658 Our study revealed a link between m^6Am and transcription. This effect was detectable because
659 of the highly quantitative nature of m^6Am measurement in CROWN-seq. Although all A-TSNs
660 show high stoichiometry, there are differences in the overall m^6Am stoichiometry between
661 transcripts, e.g., ~0.85 stoichiometry vs. 0.95 stoichiometry which can readily be detected by
662 CROWN-seq. We found that these differences are often related to the specific TSS motif. For
663 example, the Inr-like $SSCA_{+1}GC$ TSS motif was associated with the highest m^6Am
664 stoichiometry, while transcripts using the $VA_{+1}RR$ TSS motif exhibited relatively lower m^6Am
665 stoichiometry. This finding highlights that the major role of m^6Am might be linked to transcription
666 regulation, which is supported by a recent study by An et al.[39].
667
668 We then examined the effects of PCIF1 depletion on m^6Am transcript abundance. We found
669 that transcripts with higher methylation in wild-type cells tend to have a larger reduction in RNA
670 expression level upon *PCIF1* knockout. Further analysis showed that transcripts that use the
671 $SSCA_{+1}GC$ TSS motif exhibited significantly reduced expression in *PCIF1* knockout cells. In
672 contrast, transcripts that use the $VA_{+1}RR$ TSS motif were largely unaffected. Notably, transcripts
673 normally have small differences in methylation (i.e., methylation level at 0.9 vs 0.98). Thus,
674 m^6Am is unlikely to be a general stabilization mark in mRNA since it only affects transcripts
675 based on promoter sequences. Instead, these different stoichiometries of m^6Am are likely to be
676 the consequence of different transcription mechanisms. Thus, it will be important to assess how
677 these different transcription mechanisms use m^6Am for gene expression.
678
679 PCIF1 is known to be associated with RNA polymerase II and is recruited to promoter regions
680 during transcription[28]. Thus, PCIF1 is ideally positioned to regulate transcription processes. It
681 is interesting to speculate that m^6Am may provide a mark that enhances subsequent elongation
682 and thus maintains high overall expression for transcription initiation complexes that assemble
683 on the $SSCA_{+1}GC$ TSS motif. Other transcription initiation complexes, such as those using the
684 $VA_{+1}RR$ TSS motif, may not need this mechanism. However, our data cannot provide further
685 details on whether the loss of m^6Am is related to exact mechanisms such as transcription
686 initiation selection, elongation, or premature termination. Notably, the recent study by An et al.[39]
687 suggested that the loss of m^6Am is related to enhanced premature termination and therefore
688 leads to reduced RNA 5' end expression. An et al. proposed that m^6Am can sequester PCF11, a
689 m^6Am reader, and thereby promote transcription by reducing premature transcription
690 termination[39]. However, it is still unclear whether the transcripts from the $SSCA_{+1}GC$ TSS motif
691 are indeed more preferentially bound by PCF11. To better understand how PCIF1 regulates
692 transcription, assays with transcription-start nucleotide resolution will be required.
693
694 Although m^6Am and m^6A are chemically similar, these two modifications appear to have very
695 different biological functions. It is well known that m^6A is a mark for RNA instability through the
696 recruitment of YTHDF proteins[40]. However, we find no correlation between m^6Am and RNA
697 instability. Additionally, our previous YTHDF1, YTHDF2, and YTHDF3 iCLIP studies did not

show binding at mRNAs 5' ends[41], which suggests that YTHDF proteins do not bind m^6Am. Thus, specific m^6Am-binding proteins might enable its unique functions in transcription.

Although most studies of m^6Am and PCIF1 focus on mRNAs, we find that m^6Am in snRNAs exhibit substantially higher variability and regulation than that in mRNA. Early biochemical studies of snRNA composition demonstrated that the first nucleotide was generally Am in all Pol II-derived snRNAs[10]. CROWN-seq generally supports this finding since most snRNAs have low m^6Am stoichiometry. However, the previous study mainly focused on HEK293T cells[10], which have very low m^6Am in snRNA. In this study, nine different cell types were sequenced. These cell lines showed highly variable m^6Am in snRNA. In some cases, several snRNAs can reach m^6Am stoichiometry up to 0.70-0.89. These data raise the possibility that m^6Am may affect snRNA functions, such as splicing and gene transcription[12,42], and *PCIF1* knockout phenotypes may be due to altered snRNA.

Notably, m^6Am in snRNA is highly regulated by FTO, which is consistent with our earlier findings[10]. However, the previous study did not have transcript isoform level resolution in analyzing the effect of FTO demethylation. With CROWN-seq, we find that FTO has markedly different effects on different snRNAs, where some snRNAs appear highly demethylated by FTO while others are insensitive to FTO. Some snoRNA, and snRNA/snoRNA pseudogenes are also demethylated by FTO. Notably, FTO depletion affects numerous aspects of cell function[43]. Our results thus raise the possibility that FTO-depletion phenotypes may result from increased m^6Am levels in snRNAs, snoRNAs, or their pseudogenes.

Limitations of the study

One limitation of CROWN-seq is that it can be difficult to align sequencing reads to the genome. Unlike normal reads, which contain A, G, C, and U, most reads in CROWN-seq comprise only G, C, and U due to the conversion of A's. This makes it difficult to align reads to highly similar genes, such as snRNA isoforms and pseudogenes which have very similar 5' ends. For this reason, only a small fraction of reads from snRNA and pseudogenes were uniquely mapped to one genomic location and were used in this analysis. To better understand m^6Am in these 5' ends with similar sequences, future optimization is desired to increase the read lengths, which can help distinguish these sequences from each other. This requires technical innovations in reducing RNA fragmentation during sodium nitrite conversion, which comes from acid-catalyzed depurination and backbone cleavage[21].

In this study, we quantified m^6Am in nine different cell lines, which cover a wide range of PCIF1 expression levels. Although we found high m^6Am stoichiometries in all cell lines, it is possible that some cells or tissues have more variable m^6Am levels. In our previous study, mass spectrometry showed that the CCRF-SB cell line has relatively low m^6Am stoichiometry at ~67.6%[1]. However, these cells exhibit very slow growth as reported previously[1]. As a result, we were unable to obtain enough amounts of mRNA needed for CROWN-seq. Future CROWN-seq studies may lead to the identification of cell types or contexts with dynamic m^6Am landscapes.

742 The last limitation of this study is that the focus of this study was to quantify m^6Am and to predict
743 potential functions using *PCIF1* knockout cells. However, it is possible that PCIF1 has non-
744 catalytic functions that may contribute to the *PCIF1* knockout phenotype. Future experiments
745 using catalytic-dead PCIF1 can be useful to distinguish between the catalytic and non-catalytic
746 functions of PCIF1.
747
748 **ACKNOWLEDGEMENTS**
749 We thank members of the Jaffrey lab for their comments and suggestions throughout the
750 duration of this project. We thank members of the Genomics core facility at Weill Cornell
751 Medicine. This work is supported by NIH grants R35 NS111631, S10 OD030335, RM1
752 HG011563, and MH121072 (S.R.J.).
753
754 **AUTHOR CONTRIBUTIONS**
755 J.F.L., B.R.H., and S.R.J. designed the experiments. J.F.L., B.R.H., and L.N. performed
756 experiments. J.F.L. and B.R.H. analyzed experimental data. J.F.L and S.R.J. wrote the
757 manuscript.
758
759 **DECLARATION OF INTERESTS**
760 S.R.J is a scientific founder of, advisor to, and/or owns equity in Chimerna Therapeutics,
761 Lucerna Technologies, and 858 Therapeutics.
762
763 **FIGURE LEGENDS**
764
765 **Figure 1. Many m^6Am genes are mistakenly annotated.**
766
767 **(A)** Genes tend to have multiple TSSs. Shown is a histogram displaying the number of TSSs
768 per protein-coding gene in HEK293T cells. TSSs (87,624 TSSs from 9,199 genes) were
769 mapped using ReCappable-seq. These TSSs have expression levels ≥1 TPM (transcription-
770 start nucleotide per million).
771
772 **(B)** and **(C)** Examples of genes that were mistakenly classified by previous studies[14]. *SRSF1*
773 **(B)** was previously designated as m^6Am because of the miCLIP signals overlapping with A-
774 TSSs. However, based on ReCappable-seq, ~41.5% of the reads are mapped to non-A-TSSs
775 in *SRSF1*. Notably, one of the most expressed m^6Am A-TSS (chr17:58,007,228) was mistakenly
776 considered as internal m^6A because this position was not previously annotated as a TSS[44].
777 *ADAR* **(C)** was previously classified as Gm. There is no m^6Am signal based on miCLIP[14], m^6Am-
778 seq[11], or m6ACE-seq[12] mapped to *ADAR*. However, ~71% of the transcripts from *ADAR* are A-
779 initiated.
780
781 **(D)** Previously classified m^6Am genes express considerable levels of non-A-initiated transcripts.
782 Each column represents a gene previously classified as m^6Am gene by miCLIP[14]. For each
783 gene, the percentage of transcript isoforms starting with m^6Am/Am (in green) or Gm/Cm/Um (in
784 gray) are shown. The percentage was calculated by weighting each transcript isoform by its

785 expression level. The TSN frequencies were obtained using ReCappable-seq in HEK293T
786 cells.
787
788 **Figure 2. CROWN-seq correctly maps and quantifies m^6Am.**
789
790 **(A)** Schematic of CROWN-seq. RNAs are firstly treated with sodium nitrite, which causes Am at
791 the transcription-start position to be converted to Im. To isolate the TSN, m^7G caps are replaced
792 with 3'-desthiobiotin (DTB) caps. These DTB caps are enriched on streptavidin beads, while
793 uncapped background RNA fragments are uncapped and washed away. After washing, an
794 enriched pool of transcript 5' ends is released from the beads by cleaving the triphosphate
795 bridge, leaving 5' monophosphate ends that are ligated to an adapter. After adapter ligation,
796 cDNA was synthesized and amplified for Illumina sequencing. During sequencing, the
797 converted sequences were aligned to a reference genome. The TSNs can be determined as the
798 first base immediately after the 5' adapter sequence. To quantify m^6Am stoichiometry, we count
799 the number of A (m^6Am) and G (Am) bases at the TSN position.
800
801 **(B)** CROWN-seq enriches reads that contain the TSN. The relative coverage of reads mapped
802 to the TSS and non-TSS regions across the m^7G-ppp-Am-initiated RNA standard was
803 calculated. The average relative coverage of reads that map to the TSS and to non-TSS
804 positions are shown for three replicates. The 95% CI of the relative coverages is shown using
805 error bars.
806
807 **(C)** CROWN-seq exhibits high quantitative accuracy for measuring m^6Am stoichiometry. RNA
808 standards (**Table S2**) were prepared with 0%, 25%, 50%, 75%, and 100% m^6Am stoichiometry.
809 To make m^6Am standards in different m^6Am levels, we generated both Am transcripts and
810 m^6Am transcripts by *in vitro* transcription with cap analogs m^7G-ppp-Am and m^7G-ppp-m^6Am.
811 Five transcripts were made in the Am and m6Am form and mixed to achieve the indicated m^6Am
812 stoichiometry. These transcripts have identical 5' ends and different barcodes (**Table S2**).
813 Linear least-squares regression was performed to calculate the correlation between expected
814 non-conversion rates and the observed average non-conversion rates for each standard. All
815 TSNs shown in this plot have high sequencing coverage, ranging from 656 to 21,545 reads.
816
817 **(D)** CROWN-seq results for *SRSF1*. CROWN-seq shows that 54.0% of *SRSF1* transcripts
818 initiate with A. Among the A-initiated transcripts, 93.4% were resistant to conversion (A's, shown
819 in green), and therefore m^6Am. As a result, *SRSF1* has 50.4% m^6Am transcripts, 3.6% Am
820 transcripts, and 46.0% non-A-initiated transcripts. Notably, a previous miCLIP study identified
821 an internal m^6A site[44] which we found was m^6Am at the TSN based on CROWN-seq.
822
823 **(E)** CROWN-seq results for *JUN*. CROWN-seq shows that ~58% of *JUN* transcripts initiate with
824 A. Unlike *SRSF1* which A-TSNs are highly methylated, *JUN* A-TSNs are only ~75%
825 methylated. As a result, *JUN* has 43.5% m^6Am transcripts, 14.5% Am transcripts, and 42%
826 non-A-initiated transcripts.
827

828 **(F)** CROWN-seq identifies most m^6Am sites identified in previous studies. 7,480 m^6Am sites in
829 HEK293T cells found either by miCLIP[14], m^6Am-seq[11], or m6ACE-seq[12] were analyzed. The
830 high-confidence sites in CROWN-seq were defined as A-TSN with ≥20 unique mapped reads.
831 The results shown are from HEK293T cells, which is the same cell line used in all previous
832 studies. Among the 1,284 sites uniquely found in other studies, 811 sites are also mapped by
833 CROWN-seq but at lower coverage (1-19 reads); 319 sites are mapped very far (>100 nt) away
834 from any TSS annotation and thus can be considered as false positives; the remaining 154 sites
835 are mapped very closely to known TSSs and may be false negative results in CROWN-seq.
836
837 **(G)** Many A-TSNs identified in CROWN-seq in HEK293T cells are not annotated. In this
838 analysis, A-TSSs in **(F)** were intersected with the TSS annotation in Gencode v45. Only 12.2%
839 of A-TSSs found by CROWN-seq are previously annotated.
840
841 **(H)** CROWN-seq exhibits high accuracy in TSN discovery. In this analysis, we compared the
842 non-conversion of A-TSNs between wild-type and *PCIF1* knockout cells. For the 6,457 A-TSNs
843 annotated by Gencode v45, most of them have high non-conversion rates in wild-type cells and
844 very low non-conversion rates in *PCIF1* knockout cells, indicating correct TSN mapping. Similar
845 to the annotated TSNs, 25,435 newly found A-TSNs were also found to have differential m^6Am
846 between wild-type and *PCIF1* knockout. Thus, these newly found A-TSNs were also mostly true
847 positives. In this analysis, only A-TSNs mapped by at least 20 reads in both wild-type and
848 *PCIF1* knockout HEK293T cells were used. The details of these sites can be found in **Table S3**.
849
850 **(I)** The previously identified m^6Am sites are biasedly in higher expression and higher m^6Am
851 stoichiometry. Shown are the sequencing coverage (left) and non-conversion rates (right) of
852 different sets of m^6Am sites in HEK293T CROWN-seq data. In total, 98,147 sites found by
853 CROWN-seq, 2,129 sites found by miCLIP[14], 3,693 sites found by m6ACE-seq[12], and 1,610
854 sites found by m^6Am-seq[11] are shown.
855
856 **(J)** CROWN-seq has much higher sensitivity in m^6Am discovery than all existing m^6Am mapping
857 methods. In this analysis, sensitivity is defined as m^6Am/A-TSN found per million mapped reads.
858 For CROWN-seq, sensitivity was defined as the slope of linear regression result between
859 sequencing depth and A-TSN number among different samples in this study (see **Figure S2G**).
860 For other methods, sensitivity was defined as the number of reported m^6Am sites over the
861 number of reads in all libraries required for m^6Am identification.
862
863 **Figure 3. CROWN-seq reveals m^6Am landscape in mRNA.**
864
865 **(A)** Boxplot showing the overall mRNA m^6Am levels (i.e., m^6Am stoichiometry) among different
866 cell lines. The exact m^6Am levels of the mRNA m^6Am sites in this analysis can be found in
867 **Table S3**. Only m^6Am sites with ⩾50 reads mapped in at least one cell line were analyzed.
868
869 **(B)** mRNA m^6Am stoichiometry is positively correlated with PCIF1 expression. In this plot,
870 *PCIF1* expression was estimated by the number of reads mapped to *PCIF1* TSSs. The read
871 counts were normalized into transcription-start nucleotide per million (TPM) for gene expression

872 comparison. Three cell lines (CCD841 CoN, HCT-116, and HT-29) whose *PCIF1* expression
873 was estimated by western blots and RT-qPCR by Wang *et al.* [5] are highlighted. Pearson's r and
874 p-value in this analysis were obtained by linear regression.
875
876 **(C)** Overall mRNA m^6Am stoichiometry is not correlated with CTBP2 expression. Similar to **(B)**,
877 *CTBP2* expression was estimated by CROWN-seq. Four cell lines with very low *CTBP2*
878 expression are highlighted.
879
880 **(D)** Some A-TSNs have relatively low and more variable m^6Am stoichiometry among cell lines.
881 In this plot, the variability of the m^6Am stoichiometry of a site, which is defined as the maximum
882 m^6Am subtracted by the minimum m^6Am stoichiometry among all cell lines is shown on the X-
883 axis; the average m^6Am level of a site among all cell lines is shown on the Y-axis. Several
884 example genes are indicated in different colors.
885
886 **(E)** Boxplots and dotplots showing the m^6Am levels of different A-TSNs in *JUN*, *ENO1*, *MYC*,
887 and *ACTB*. These genes contain A-TSNs with relatively low m^6Am stoichiometry. In this plot, the
888 exact m^6Am levels of individual A-TSNs are shown in dots, while the median and IQR of the
889 m^6Am levels are shown in boxplots. Only m^6Am sites with ≥50 reads mapped were analyzed.
890
891 **(F)** Gene Ontology enrichment (Cellular Components) of genes containing lowly methylated
892 m^6Am sites. The full Gene Ontology results can be found in **Table S4**.
893
894 **(G)** A-TSNs in histone genes tend to have relatively low m^6Am stoichiometry. In this plot,
895 histone genes are categorized by their genomic localizations. Histone gene cluster 6p22.1-2
896 and 1q21.1-2 are the two major histone gene clusters. For histone gene cluster 6p22.1-2, 55 to
897 173 A-TSNs are shown in different cell lines; for histone gene cluster 1q21.1-2, 9 to 14 A-TSNs
898 are shown; for other histone genes, 24 to 109 A-TSNs are shown.
899
900 **Figure 4. m^6Am stoichiometry is related to core promoter sequence.**
901
902 **(A)** m^6Am stoichiometry is related to base composition in both upstream and downstream of A-
903 TSNs. In these plots, 58,723 A-TSNs are grouped into twenty 5-percentile bins (X-axis). For
904 each bin, the frequency of A, T, C, and G bases at each position relative to the A-TSN are
905 plotted on the Y-axis. Among different positions in the promoter region, C's in -4, -1, and +3, as
906 well as G's in +2 are positively correlated with high m^6Am; while A's in +2 are negatively
907 correlated with high m^6Am. Results for other promoter positions can be found in **Figure S4A**.
908
909 **(B)** Motif analysis of A-TSNs with the lowest 5% m^6Am stoichiometry (upper) and the A-TSNs
910 with the highest 5% m^6Am stoichiometry (lower). The core promoter region (-40 to +41) was
911 screened for enriched motifs. The lowest 5% A-TSNs exhibited a $VA_{+1}RR$ TSS (V=A/C/G,
912 R=A/G) motif, while the highest 5% A-TSNs exhibited a $SSCA_{+1}GC$ (S=C/G) motif. The
913 sequence contexts for all A-TSNs are shown in **Figure S3E**.
914

915 **(C)** A-TSNs expressed from different core promoters exhibit different m^6Am stoichiometry. Core
916 promoters containing the $VA_{+1}RR$ motif produce transcripts with relatively low m^6Am
917 stoichiometry. Transcripts using the $SSCA_{+1}GC$ motif exhibited relatively high m^6Am
918 stoichiometry. In comparison, the m^6Am stoichiometry in conventional A-TSNs from either
919 $BBCA_{+1}BW$ or BA_{+1} is also shown and exhibits intermediate m6Am stoichiometry. In this
920 analysis, 14,788, 7,981, 34,578, and 1,376 A-TSNs were used for each of the four motifs. P-
921 values, Student's t-test, two-sided.
922
923 **(D)** TATA-box containing core promoters exhibit relatively low m^6Am stoichiometry. For this
924 analysis, the TATA-box is defined as TATAWAWR[29]. Because many TATA-boxes found in our
925 A-TSN dataset are outside the classic -31 to -24 region, we extended the region for the TATA-
926 box search to -36 to -19. Since histone genes preferentially contain TATA box, we separately
927 plotted TATA-box-containing histone genes (N=155) and TATA-box-containing non-histone
928 genes (N=28). 58,540 A-TSNs without TATA-box are also shown. P-values, Student's t-test,
929 two-sided.
930
931 **Figure 5. *PCIF1* knockout leads to m^6Am and TSS motif-related A-TSN expression**
932 **changes.**
933
934 **(A)** m^6Am stoichiometry is positively related to A-TSN expression in wild-type HEK293T cells. In
935 this cumulative distribution plot, the expression of each A-TSN was quantified by ReCappable-
936 seq, for all A-TSNs in each indicated m^6Am stoichiometry bin. A-TSNs (n=58,723) were
937 grouped into five bins based on m^6Am stoichiometry quantified by CROWN-seq. In total, 5,125,
938 6,962, 7,991, 8,368, and 8,009 A-TSNs are shown in each bin (from low m^6Am to high m^6Am).
939 These A-TSNs have an average TPM ≥1 in two ReCappable-seq replicates and coverage ≥50
940 in CROWN-seq. P-values, Student's t-test for TPM (log-transformed), two-sided.
941
942 **(B)** The expression level of high m^6Am stoichiometry A-TSNs is reduced in *PCIF1* knockout.
943 Shown is a cumulative distribution plot of A-TSN expression change in HEK293T cells upon
944 *PCIF1* knockout. The differential expression of A-TSN was calculated by DESeq2[45]. Similar to
945 **(A)**, the A-TSNs were binned based on the m^6Am stoichiometry. In total, 3,269, 2,272, 3,218,
946 3,813, and 3,369 A-TSNs are shown in each bin (from low m^6Am to high m^6Am). A-TSNs with a
947 baseMean (i.e., the average of the normalized count among replicates) ≥100 were used in the
948 differential expression test (two replicates were used for both wild-type and *PCIF1* knockout)
949 and coverage ≥50 reads in CROWN-seq. P-values, Student's t-test, two-sided.
950
951 **(C)** Shown are cumulative distribution plots of expression changes of A-TSNs and G-TSNs after
952 PCIF1 depletion. 14,516 A-TSNs and 9,667 G-TSNs with expression levels quantified by
953 ReCappable-seq are shown. These A-TSNs and G-TSNs have baseMean ≥100 during the
954 differential expression test. P-values, Student's t-test, two-sided.
955
956 **(D)** Similar to **(B)**, A-TSNs that use different TSS motifs exhibit different changes in expression
957 upon *PCIF1* knockout. In total, 352 A-TSNs using $SSCA_{+1}GC$, 7,928 A-TSNs using BA_{+1}, 2,958
958 A-TSNs using $BBCA_{+1}BW$, and 2,760 A-TSNs using $VA_{+1}RR$ are shown. These A-TSNs have

959 baseMean≥100 during differential expression test (2 replicates for both wild-type and *PCIF1*
960 knockout) and coverage ≥50 reads in CROWN-seq. P-values, Student's t-test, two-sided.
961
962 **Figure 6. CROWN-seq reveals m^6Am landscape in snRNA and snoRNA.**
963
964 **(A)** Heatmaps showing m^6Am stoichiometry in different snRNA gene families and isoforms. Cell
965 lines in the column are ranked by the overall mRNA m^6Am stoichiometry. The name of each
966 snRNA isoform is shown on the right. A-TSNs already annotated in Gencode v45 are
967 highlighted in bold. For newly found A-TSNs, the relative distance between the new A-TSN and
968 the nearest annotated A-TSN is showed in brackets. Note that Gencode v45 contains snRNA
969 annotation from different databases. For example, *RNU1-4* and *U1.22* are both U1 snRNA,
970 however, *RNU1-4* is from the HGNC database and *U1.22* is from the RFAM database.
971
972 **(B)** Similar to **(A)**, Heatmaps show the m^6Am stoichiometry in different snoRNA isoforms.
973
974 **(C)** and **(D)**, snRNA methylation levels are not well correlated with *PCIF1* expression, but
975 negatively correlated with *FTO* expression. The RNA expression levels of *PCIF1* and *FTO* were
976 estimated by reading counts in CROWN-seq, which were converted into TPM to normalize the
977 sequencing depth. Linear regressions were performed to obtain Pearson's r and p-value of the
978 correlations.
979
980 **(E)** FTO depletion leads to increased m^6Am level (i.e., m^6Am stoichiometry) in many kinds of
981 snRNA and snoRNA. In this plot, the difference in m^6Am levels between wild-type and *FTO*
982 knockout cells is shown in the first row. The exact m^6Am levels in *FTO* knockout and wild-type
983 cells are shown in the second and third rows. Different kinds of snRNA and snoRNA are shown
984 in different colors.
985
986 **(F)** FTO depletion leads to increased m^6Am stoichiometry in snRNA and snoRNA pseudogenes.
987 In this plot, shown are the annotated pseudogenes of U1, U2, U4, U5, and 7SK, as well as the
988 newly identified snRNA/snoRNA pseudogenes in intronic and intergenic regions. Several
989 mRNAs exhibited 5' ends resembling snRNA pseudogenes. However, these snRNA-like mRNA
990 5' ends showed high and stable m^6Am stoichiometry in both wild-type and *FTO* knockout cells.
991
992 **SUPPLEMENTAL TABLES**
993
994 **Table S1.** Comparison of m^6Am mapping methods.
995
996 **Table S2.** The design of m^6Am standards.
997
998 **Table S3.** mRNA m^6Am stoichiometry in different cell lines.
999
1000 **Table S4.** Gene Ontology enrichment of genes with relatively low m^6Am sites.
1001

1002 **Table S5.** Comparing A-transcription-start nucleotide expression between wild-type and *PCIF1*
1003 knockout cells.
1004
1005 **Table S6.** m^6Am stoichiometry of A-TSN in snRNA, snoRNA, and pseudogenes.
1006
1007 **Table S7.** Oligos used in this study.
1008
1009 **METHODS**
1010
1011 **EXPERIMENTAL MODEL AND SUBJECT DETAILS**
1012
1013 **Cell lines**
1014 HEK293T (wild-type, *PCIF1* knockout, and FTO knockout cells), A549 (wild-type and *PCIF1*
1015 knockout), HCT-116, Huh-7, and HT-29 cells were maintained in DMEM (Gibco #11995065).
1016 HepG2 and CCD841 CoN cells were maintained in EMEM (ATCC #30-2003). K562 and Jurkat
1017 E6.1 cells were maintained in RPMI1640 (Gibco #11875093). All media was supplemented with
1018 10% FBS and 1X penicillin-streptomycin (Gibco #15140148). Cells were grown at 37 °C with 5%
1019 CO_2. We followed the instructions from the manufacturer to maintain the cells.
1020
1021 **METHODS DETAILS**
1022
1023 **RNA extraction and mRNA purification**
1024 Cellular total RNA in TRIzol LS (ThermoFisher #10296028) was extracted by Direct-zol RNA
1025 Miniprep kit (Zymo #R2070) or by Phenol Chloroform extraction. mRNA was purified by
1026 NEBNext Oligo d(T)25 Beads (NEB #E7499) or Dynabeads Oligo (dT)25 (Ambion #61002)
1027 based on mRNA purification from total RNA protocol of Dynabeads Oligo (dT)25 (Ambion
1028 #61002).
1029
1030 **m^6Am standard preparation**
1031 We used *in vitro* transcription to prepare m^7G capped m^6Am- or Am-initiated transcripts, which
1032 are based on HiScribe® T7 mRNA Kit with CleanCap® Reagent AG (NEB #E2080S). We first
1033 obtained DNA templates from IDT gBlock. In total, five DNA templates which are identical
1034 expect for the 6-nt long barcode 42-nt downstream to the TSS were used (**Table S2**). The DNA
1035 templates contain 5'-TAATACGACTCACTATAAG-3' T7 promoter for *in vitro* transcription. We
1036 used CleanCap® Reagent AG (3' OMe) (TriLink #N-7413), which is included in NEB #E2080S,
1037 to generate m^7G-ppp-Am modified transcripts. We used CleanCap® Reagent M6 (TriLink #N-
1038 7453) to generate the m^7G-ppp-m^6Am modified transcripts. The RNAs made by *in vitro*
1039 transcription were DNase I treated, purified, and then quantified by both Agilent TapeStation
1040 (RNA high sensitivity assay). We then mixed the Am and m^6Am modified oligos to generate
1041 m^6Am standards with expected m^6Am stoichiometry at 0%, 25%, 50%, 75%, and 100% m^6Am
1042 stoichiometry. Notably, the guaranteed purity of the CleanCap® Reagent M6 is >95%. The
1043 CleanCap® Reagent M6 can contain m^7G-ppp-AmG analog, which results in the reduced non-
1044 conversion rate in CROWN-seq.
1045

1046 **Genomic assembly and annotations**
1047 The genomic sequence and annotations of Gencode v45 primary assembly were used in this
1048 study.
1049
1050 **GLORI experiment**
1051 To validate whether sodium nitrite conversion can convert Am into Im, we spiked ~0.01 ng Am
1052 transcripts (ERCC-00057-1-TCGTCG) into ~250 ng poly(A) selected mRNA for GLORI assay.
1053 Ligation-based GLORI protocol was used in this study. Notably, the Am transcripts were
1054 decapped by mRNA Decapping Enzyme (NEB #M0608S) in advance. We first fragmentized the
1055 input RNA into ~200 nt long fragments (NEBNext Magnesium RNA Fragmentation Module (NEB
1056 #E6150S), 94°C, 2 minutes). The fragmentized RNAs were then A-to-I converted based on the
1057 GLORI protocol[20]: we converted the glyoxal-protected RNA by 750 mM $NaNO_2$ at 16°C for 8
1058 hours and 4°C overnight. The RNA was then deprecated in a deprotection buffer at 95°C for 10
1059 minutes. The deprotected RNA was then T4 PNK (NEB #M0210S) treated and processed to
1060 ligation-based small RNA-seq library preparation[46]. Notably, the 5' adapter in library preparation
1061 contains an 11 nt UMI sequence (see **Table S7**).
1062
1063 **GLORI data processing**
1064 GLORI libraries were analyzed based on a modified mRNA bisulfite sequencing pipeline[47]. The
1065 first 10 bases in GLORI libraries made with eCLIP protocol were first extracted by a customized
1066 script. GLORI reads were first quality trimmed by Cutadapt[48]. For the GLORI library generated
1067 by eCLIP protocol, the parameters are --max-n 0 --trimmed-only -a
1068 AGATCGGAAGAGCGTCGTG -e 0.1 -q 30 -m 40 --trim-n; for GLORI library prepared by ligation
1069 based protocol generated in this study, the parameters are -m 32 -j 4 -q 20 -e 0.25 -a
1070 AGATCGGAAGAGCACACGTC -A ATATNNNNNNNNNNNAGATCGGAAGAGCGTCGTG. After
1071 pre-processing, the reads were firstly A-to-G converted and aligned to A-to-G (positive strand)
1072 and T-to-C (negative strand) converted reference genome and transcriptome by Hisat2-2.1.0[49].
1073 Parameters in alignment: -k 5 –fr –rna-strandness FR –no-temp-splicesite –no-mixed. Only
1074 unique alignments were used. After alignment, the base information in sequences was restored
1075 so that m^6Am signals can be reflected by the A-to-G mismatches. No further transcriptome
1076 alignment was performed on the unmapped reads. After alignment, a customized script based
1077 on Pysam[50] was used to pileup every single base to obtain the A, C, G, and U counts. Every
1078 single base was assigned to a transcript isoform if possible (order: mRNA > lncRNA > functional
1079 RNAs > pseudogenes). Non-conversion rate is defined as the number of A counts against the
1080 sum of A count and G count. Filters were applied to obtain high-quality non-converted A
1081 (m^6A/m^6Am) signals in a gene-specific manner: (1) only genes with at least 1000 counts were
1082 analyzed; (2) gene-specific non-conversion rates were computed for Binomial test on the
1083 frequency of non-conversion and sites with Binomial test P-value < 0.05 were used; (3) reads
1084 with more than 3 non-converted As were considered as noise and discarded; (4) sites with more
1085 than 5% signals were discarded due to the site may fall in a conversion-resistant region; (5)
1086 Only sites with no less than 20 reads covered and non-conversion rates over 0.1 were
1087 considered as m^6A/m^6Am sites. (6) Non-conversion rates of the same site from different
1088 replicates were averaged. Details of this pipeline can be found at
1089 https://github.com/jhfoxliu/GLORI_pipeline.

1090
1091 **ReCappable-seq library preparation**
1092 A modified ReCappable-seq protocol[18] was developed to reduce background, reduce material
1093 loss, and increase the utility of mapped reads. Several steps of library construction are now
1094 performed while the 5' desthiobiotinylated cap is bound to streptavidin beads. This reduces the
1095 opportunity for carry-through of random fragmentation products to occur that would previously
1096 result in non-cap-derived 5' ends to be ligated. Next, 5' adapters with unique molecular indexes
1097 (UMIs) are used to permit robust PCR duplicate removal. Finally, ~160 spike-in mRNAs from
1098 SIRV-ERCC Spike-in mixture (Lexogen #051.03) with single defined 5' termini are used, which
1099 are used during analysis to build a dynamic thresholding pipeline that exclude false positive
1100 start sites. A complete step-by-step protocol as performed here will be available on the
1101 accompanying GitHub page (see **Data and Code Availability**).
1102
1103 5 µg total RNA was used as input for all experiments. RNA was denatured at 65 °C for 2
1104 minutes before reaction mixes were added. First, 5'-phosphorylated RNAs were
1105 dephosphorylated using 25 U Quick CIP (NEB #M0525L) in a 50 µL reaction for 30 minutes at
1106 37 °C. The reaction was cleaned using a Zymo RCC-5 column following the
1107 manufacturer's >200 nt protocol and eluted with 20 µL water. m^7G capped RNAs were then
1108 decapped using 200 U yDcpS (NEB #M0463S) for 1 hour at 37 °C. This unique decapping
1109 enzyme liberates m^7GMP, resulting in mRNAs with a 5'-diphosphate. The reaction was cleaned
1110 and eluted as before. Next, the 5'-diphosphorylated mRNAs were recapped with desthiobiotin-
1111 GTP (DTB-GTP) using vaccinia capping enzyme (5 µL VCE buffer, 0.5 µL inorganic
1112 pyrophosphatase (NEB #M0361S), 5 µL DTB-GTP (5 mM; NEB #N0761S), 50 U VCE
1113 (#M2080S)) for 45 minutes at 37 °C. The reaction was clean as before, however, a total of 4
1114 washes were performed to ensure the complete removal of excess DTB-GTP. RNA was then
1115 fragmented by incubating at 95 °C for 2.5 minutes in a 25 µL reaction containing 100 mM Tris-
1116 HCl pH 8.0 and 2 mM $MgCl_2$. Fragmented RNA was placed on ice and brought to 30 µL with
1117 water. Streptavidin beads (NEB #S1421S) were washed in a high salt wash buffer (10 mM Tris-
1118 HCl pH 7.5, 2 M NaCl, 1 mM EDTA) and resuspended in the high salt buffer at 4 mg/mL. 30 µL
1119 beads were added to 30 µL fragmented RNA and incubated for 45 minutes at room temperature
1120 with agitation. Beads were washed twice in a high salt buffer, twice in a lower salt buffer (10 mM
1121 Tris-HCl pH 7.5, 250 mM NaCl, 1 mM EDTA), and twice in PNK wash buffer (20 mM Tris-HCl
1122 pH 7.5, 10 mM $MgCl_2$, 0.2% Tween). Beads were next resuspended in 40 µL PNK reaction mix
1123 (8 µL 5X pH 6.5 PNK buffer (350 mM Tris-HCl pH 6.5, 50 mM $MgCl_2$, 5 mM DTT), 1 µL T4 PNK
1124 (NEB #M0201S), 1 µL RNaseOUT (ThermoFisher #10777019) and incubated at 37 °C for 30
1125 minutes with agitation to remove 3' phosphates resulting from the fragmentation. Beads were
1126 washed once in PNK wash, once in the high salt wash, then twice again in PNK wash. Next, a 3'
1127 adapter (see **Table S7**) was added to RNA by resuspending beads in 40 µL 3' ligation reaction
1128 mix (4 µL T4 RNA ligase buffer, 2 µL T4 RNA ligase 2 truncated KQ (NEB #M0373L), 1 µL
1129 RNaseOUT, 2 µL L7 adapter (20 µM stock, see **Table S7**), 16 µL of 50% PEG-8000) and
1130 incubated at 25 °C for 2 hours. The beads were washed once in PNK wash, once in high salt
1131 wash, twice in lower salt wash, then resuspended in 30 µL lower salt wash containing 1 mM
1132 biotin (ThermoFisher #B20656) to elute DTB-capped RNA fragments. The eluted RNA was
1133 cleaned by ethanol-AMPure XP (1.8 volumes AMPure XP, then 1.5 volumes 100% ethanol). To

increase stringency, the streptavidin bead enrichment was repeated omitting enzymatic steps and instead washing three times with high salt and then three times with lower salt wash, and the eluate was cleaned again by ethanol-AMPure XP. The DTB-GTP cap was removed using 0.5 U/µl RppH (NEB #M0356S) in 1X ThermoPol buffer (NEB #M0356S) and incubating at 37 °C for 1 hour. The resulting 5'-monophosphate RNA fragments were purified by ethanol-AMPure XP. 30 pmol of a 5' adapter was ligated for 3 hours at 25 °C with 2 U/µL T4 RNA ligase 1 (NEB #M0437M). This RNA adapter contains an 11 nt UMI followed by a fixed sequence (AUAU) at its 3' end. The UMI allows robust duplicate removal, and the fixed sequence provides an anchor point to correctly identify the first nucleotide of the mRNA. The ligation reaction was inactivated by heating at 65 °C for 10 minutes and then immediately used in a reverse transcription reaction. 3 pmol of ReCappable-seq RT primer was annealed to the 3' adapter of RNA fragments by heating to 65 °C for 5 minutes and cooling to 25 °C at a rate of 0.1 °C/sec. Reverse transcription was carried out at 55 °C for 45 minutes in a reaction containing 0.5 mM dNTPs, 5 mM DTT, 20 U RNaseOUT, 50 mM Tris-HCl pH 8.3, 75 mM KCl, and 300 U SuperScript III (ThermoFisher #18080044). Following heat inactivation, the reaction was cleaned using ethanol-AMPure XP and cDNA was resuspended in 21 µL. The final PCR was performed using 8 µL cDNA in a 40 µL reaction containing 1X Phusion HF master mix (NEB #M0531L) and 4 µL each of a unique i5 and i7 barcoded primer combination for each sample (NEB #E7600S). Cycling conditions were typically 98 °C 2 minutes, then 11-13 cycles of 98 °C 15 seconds, 65 °C 30 seconds, 72 °C 30 seconds, with a final 5 minute 72 °C extension. The optimal number of cycles for each library was determined by performing a set of test cycles using 1 µL cDNA in a 20 µL reaction. PCR libraries were purified with 2 rounds of bead clean-up using 0.9X volume SPRIselect beads. Libraries were pooled at equimolar concentrations and sequenced in paired-end mode with 50-150 bp reads depending on the library on either an Illumina NovaSeq, NextSeq, or HiSeq (please refer to GEO accession for specific details for each library).

ReCappable-seq analysis

The beginning of read 1 is the UMI plus an ATAT spacer sequence, and the nucleotide directly following this is the TSS. Reads were first filtered to identify pairs with the correct UMI+ATAT sequence, then the UMI was added to FASTQ headers using UMI-tools v1.1.1[51]. ATAT sequence discarded. Adapters were trimmed using Cutadapt v3.4[48]. Next, reads mapping to ribosomal RNA and small non-coding RNAs were filtered away by aligning to these sequences using bowtie2 v2.4.2[52]. Reads were then aligned to GRCh38 and m^6Am standard sequences using HISAT2[49]. The alignment results were deduplicated by UMI-tools (--paired --chimeric-pairs=discard --unpaired-reads=discard --method=unique). Only reads without 5' softclipping were used. A customized script based on Pysam[50] was used to extract the 5' ends from the BAM file. To annotate the sites by a gene, the 5' ends were firstly annotated by the nearest TSS within the 100 bp region. If multiple annotations were found, the annotation was selected by the priority of snRNA > snoRNA > mRNA > lncRNA > others. BEDtools v2.27.1[53] was used to find the nearest annotation. To more accurately estimate the expression levels of each TSN, we normalized the read counts using the "RUVg" function in RUVSeq pacakge[54]. To calculate the expression levels of TSNs in wide-type cells, we calculated the TPM values based on the

1177 normalized read counts. To calculate the differential expression between wild-type and *PCIF1*
1178 knockout cells, the normalized read counts were proceeded by DESeq2[45].
1179
1180 **CROWN-seq library preparation**
1181 CROWN-seq uses the glyoxal-based guanosine protection protocol from GLORI[20] and a TSN
1182 enrichment protocol that is modified from ReCappable-seq[18]. In CROWN-seq, glyoxal protection
1183 is very important to prevent both internal G's from being converted into xanthosine, which can
1184 interrupt base pairing and cause mutations during reverse transcription[55]. Because N7-methyl
1185 does not interrupt the interaction between glyoxal and N1 and N2 positions of guanosines,
1186 glyoxal protection is also very useful to prevent m^7G from being converted, which can help 5'
1187 end enrichment. After glyoxal protection, A bases are deaminated into inosines by sodium
1188 nitrite. After deamination, the 5' end RNA fragments with a m^7G cap were enriched by
1189 ReCappable-seq workflow, where the m^7G caps were replaced by a 5' desthio-biotinylated cap
1190 for enrichment by streptavidin beads. 3' adapter and 5' adapter (with unique molecular indexes
1191 (UMIs)) were ligated to the enriched 5' RNA fragments, so that the library can be made by
1192 reverse transcription followed by indexing PCR. Detailed workflow is described below.
1193
1194 Conversion. 0.8-2.5 µg oligo(dT) selected RNA was used as input. RNA was first diluted in 14 µl
1195 water. To perform glyoxal protection, 6 µl 8.8 M glyoxal and 20 µl DMSO were then added to the
1196 diluted RNA and well mixed. The 40 µl mix was first incubated at 50 ºC for 30 minutes, then 10
1197 µl boric acid was added to the mix. The 50 µl mix was then incubated for an additional 30
1198 minutes at 50 ºC. After protection, the 50 µl protected RNA was mixed with 50 µl deamination
1199 buffer (25 µl 1500 mM $NaNO_2$, 4 µl 500 mM MES, pH 6.0, 10 µl 8.8 M glyoxal, and 11 µl water).
1200 The deamination reaction was performed at 16 ºC for 8 hours. After deamination, the RNA was
1201 recovered by ethanol precipitation. To remove the glyoxal adduct from the RNA, the RNA pallet
1202 was dissolved in 50 µl deprotection buffer (500 mM TEAA pH=8.6, 47.5% deionized formamide)
1203 and was incubated at 95 ºC for 10 minutes. After incubation, the reaction was brought to 250 µl
1204 with water. Converted RNA was purified by ethanol precipitation and eluted in 39 µl water for 5'
1205 end enrichment. The converted RNA was stored at -80 ºC before 5' end enrichment.
1206
1207 Recapping. To eliminate the contamination of RNA with 5'-triphosphate and 5'-monophosphate,
1208 5 µl 10X CutSmart buffer, 5 µl Quick CIP (5 U/µl) (NEB #M0525L), and 1 µl SUPERase·In
1209 RNase inhibitor (ThermoFisher #AM2696) were added to the 39 µl converted RNA to set up a
1210 dephosphorylation reaction. The dephosphorylation reaction was performed at 37 °C for 30
1211 minutes. The reaction was cleaned up using Zymo RCC-5 column and the RNA was eluted in
1212 42 µl water. To decap the m^7G capped RNA, a 50 µl decapping reaction was set up by adding 5
1213 µl 10X yDcpS buffer, 2 µl (200 U) yDcpS (NEB #M0463S), and 1 µl SUPERase·In to the 42 µl
1214 dephosphorylated RNA. The decapping reaction was performed at 37 ºC for 1 hour. This unique
1215 decapping enzyme liberates m^7GMP, resulting in mRNAs with a 5'-diphosphate. The reaction
1216 was cleaned and eluted as before. The reaction was cleaned up using Zymo RCC-5 column and
1217 the RNA was eluted in 33.5 µl water. The 5'-diphosphorylated mRNAs were recapped with
1218 desthiobiotin-GTP (DTB-GTP, NEB #N0761S) using vaccinia capping enzyme (VCE, NEB
1219 #M2080S) (5 µL VCE buffer, 0.5 µL inorganic pyrophosphatase (NEB #M0361S), 5 µL DTB-
1220 GTP (5 mM), 50 U VCE, 1 µl SUPERase·In) at 37 °C for 1 hour. The reaction was cleaned up

using Zymo RCC-5 column and the RNA was eluted in 30 µl water. Now the RNA is ready for streptavidin enrichment.

5' enrichment. Streptavidin beads (NEB #S1421S) were washed in a high salt wash buffer (10 mM Tris-HCl pH 7.5, 2 M NaCl, 1 mM EDTA) and resuspended in the high salt buffer at 4 mg/mL. To enrich the RNA and tag the 5' and 3' end by the specific adapter, the 30 µl recapped RNA was first mixed with 30 µl streptavidin beads and incubated at room temperature for 45 minutes with agitation. Beads were washed twice in high salt buffer, twice in a lower salt buffer (10 mM Tris-HCl pH 7.5, 250 mM NaCl, 1 mM EDTA), and twice in PNK wash buffer (20 mM Tris-HCl pH 7.5, 10 mM $MgCl_2$, 0.2% Tween). To remove 3' phosphates resulting from fragmentation during conversion, beads were resuspended in 50 µl PNK reaction without ATP (5 µl 10X PNK buffer, 1 µl T4 PNK (#M0201S), 1 µl SUPERase·In, 43 µl water), and incubate at 37 °C for 30 minutes with agitation. The beads were then washed once in PNK wash buffer, once in 2 M NaCl wash, and twice in PNK wash. Next, RNA was ligated to a 74 nt-long 3' adapter (**see Table S7**) in the following 40 µl 3' ligation mix: 4 µL T4 RNA ligase buffer, 2 µl T4 RNA ligase 2 truncated KQ (NEB #M0373L), 1 µl SUPERase·In, 2 µl extended-L7 adapter (20 µM stock), 16 µl of 50% PEG-8000) and incubated at 25 °C for 2 hours. After incubation, the reaction buffer was removed by washing once with high salt buffer and twice with PNK wash buffer. To remove the exceeded adapter, the beads were incubated in 50 µl adapter digestion reaction (40 µl water, 5 µl 10X RNA ligase buffer, 1 µl RecJf (NEB #M0264S), 1 5' Deadenylase (NEB #M0331S), 1 µl SUPERase·In) at 30 °C for 15 minutes then at 37 °C for 15 minutes. The beads were washed once with PNK wash, once with high salt buffer, and twice with low salt buffer. To elute the DTB labeled RNA, beads were then suspended with 30 µl low salt wash buffer containing 1 mM free D-biotin (ThermoFisher #B20656) and incubate at room temperature for 1 hour. The DTB-labeled RNA was purified with ethanol-AMPure XP (RNA:beads:ethanol=1:2:3) and eluted in 30 µl water. To increase stringency, the streptavidin bead enrichment was repeated omitting enzymatic steps and instead washing three times with high salt and then three times with lower salt wash, and the eluate was cleaned again by ethanol-AMPure XP.

5' adapter addition. The DTB-GTP cap was removed using 0.5 U/µl RppH (NEB #M0356S) in 1X ThermoPol buffer (NEB #M0356S) and incubating at 37 °C for 1 hour. The resulting 5'-monophosphate RNA fragments were purified by ethanol-AMPure XP and eluted in 10 µl water. 1 µl (10 pmol) reverse transcription primer (see **Table S7**) was pre-annealed to the templates by heating up to 75 °C for 5 minutes, then 37 °C for 15 minutes, 25 °C for 15 minutes, and chilled at 4 °C. 10 pmol of a 5' adapter (see **Table S7**) was ligated for 3 hours at 25 °C with 2 U/µl T4 RNA ligase 1 (NEB #M0437M). This RNA adapter contains an 8 nt- or 11 nt-long UMI followed by a fixed sequence (AUAU) at its 3' end. The UMI allows robust duplicate removal, and the fixed sequence provides an anchor point to correctly identify the first nucleotide of the mRNA. 40 µl ligation product was used.

cDNA synthesis and PCR. Reverse transcription was carried out at 50 °C for 45 minutes in a 50 µl reaction containing 0.5 mM dNTPs, 5 mM DTT, 20 U RNaseOUT, 50 mM Tris-HCl pH 8.3, 75 mM KCl, and 300 U SuperScript III. To perform indexing PCR, 40 µl Phusion master mix (NEB #

1265 M0532L) was added to the reverse transcription product, along with 5 µl i5 indexing primer and
1266 5 µl i7 indexing primer (NEB #E7600S). Cycling conditions were typically 98 °C 2 minutes, then
1267 16 cycles of 98 °C 15 seconds, 65 °C 30 seconds, 72 °C 30 seconds, with a final 5 minute
1268 72 °C extension. Two rounds of 0.9X AMPureXP bead purifications were performed to remove
1269 primers. Normally ~10 ng indexed library was obtained for each library. The libraries were mixed
1270 and sequenced by NovaSeq 6000 or NovaSeqX.
1271
1272 **CROWN-seq data processing**
1273 The read pairs were firstly quality trimmed by Cutadapt[48]: -m 32 -q 20 -e 0.25 -a
1274 AGATCGGAAGAGCACACGTC. For the 8 nt-long 5' adapter, -A
1275 ATATNNNNNNNNAGATCGGAAGAGCGTCGTG was used; for the 11 nt-long adapter, -A
1276 ATATNNNNNNNNNNAGATCGGAAGAGCGTCGTG was used. Then the UMI along with the
1277 fixed ATAT spacer sequences were extracted by UMI-tools[51]. The alignment process was
1278 modified from the previous RNA bisulfite alignment strategy[47]. In brief, *in silico* converted read
1279 pairs (read1 A-to-G, read2 T-to-C) were aligned by HISAT2[49] against A-to-G converted (for
1280 positive strand) and T-to-C converted (for negative strand) reference genome and transcriptome
1281 first (key options: -k 5 –fr –rna-strandness FR –no-temp-splicesite –no-mixed). Then the unique
1282 alignments were extracted and the *in silico* converted reads were inverse-transformed to the
1283 original format. Since two sequences after conversion can be easily confused, we require the
1284 best alignment results can be well distinguished from the secondary alignments. Here, the
1285 alignment scores (AS tag in Hisat2 alignments, higher is better) of the best alignments should
1286 be higher than -10. Meanwhile, the difference between the best alignments and secondary
1287 alignments should be larger than 9. For paired-end alignments, the alignment scores of read1
1288 and read2 were summed. Only read1 was used in the 5' end analysis. Only read1 reads without
1289 5' end softclips were used. Pileup was performed to obtain the read coverages of every 5' end
1290 in the transcriptome. Non-conversion rates of the transcription start nucleotides were calculated
1291 by A counts over A and G counts.
1292
1293 To annotate the TSNs mapped in CROWN-seq, we used the TSSs in Gencode v45 as the
1294 reference TSS positions. We first calculated the distance between the mapped TSNs and the
1295 annotated TSSs by BEDtools[53]. We then tried to assign a TSN to a gene if there was an
1296 annotated TSS <100 nt away. Because there can be multiple annotations available, we used
1297 the following priority in selecting gene annotations: snRNA > snoRNA > protein-coding >
1298 lncRNA > others. We also annotated TSNs which come from RNA highly similar to snRNA,
1299 snoRNA, or their pseudogenes. To do so, we first built a BLASTn database containing all
1300 snRNA, snoRNA, and their pseudogene sequences from Gencode v45. We then performed
1301 BLASTn (BLAST 2.9.0+[56]) on the A-TSNs along with the first 50 nt downstream sequences to
1302 examine the similarity to the known snRNA, snoRNA, and pseudogenes. The following
1303 parameter was used: -qcov_hsp_perc 50 -perc_identity 50 -word_size 10. Sequences with
1304 bitscore ≥50 were considered as snRNA/snoRNA-like. We also annotated uORF and IRES
1305 elements based on ORFdb[57] and IRES atlas[58], respectively.
1306
1307 The related pipeline and scripts are available at https://github.com/jhfoxliu/CROWN-seq.
1308

1309 **RT-qPCR**
1310 1 µg total RNA was used as input. The RNA was then mixed with 1 µl Oligo dT(18) (100
1311 pmoles) (ThermoFisher #SO131), and 1 µl dNTP in 14.5 µl total volume. The mix was incubated
1312 at 65 °C for 5 minutes, then on ice for >30 seconds. After the incubation, 4 µl 5X RT mix
1313 (Maxima H- buffer, ThermoFisher #EP0751), 0.5 µl RNaseOUT (ThermoFisher #10777019),
1314 and 1 µl Maxima H- RTase were added to the mix. Reverse transcription was performed at
1315 25 °C for 10 minutes, then 50 °C for 30 minutes. After reverse transcription, 1 µl cDNA was
1316 used for qPCR. In addition to the cDNA input, the qPCR buffer contains 10 µl Power SYBR
1317 Green PCR Master Mix (ThermoFisher #368577), 0.5 µl forward primer, 0.5 µl reverse primer,
1318 and 8 µl water. qPCR was performed based on the standard quantification program in
1319 QuantStudio™ 5 System.
1320
1321 **Gene ontology analysis**
1322 Gene ontology analyses were performed with R package ClusterProfiler[59]. P-value cutoffs were
1323 set to 0.05 and q-value cutoffs were set to 0.1. “Cellular Components” and “Biological Process”
1324 terms were analyzed. Importantly, corresponding gene sets, rather than all genes, were used as
1325 the backgrounds in term enrichment computation. Since the output terms were normally
1326 redundant, terms were de-redundancy by the “simplify” function in R package GOSemSim[60]
1327 (cutoff=0.7, by="p.adjust", select_fun=min).
1328
1329 **Motif analysis**
1330 To search for the potential motifs for elements related to transcription initiation, we used “re”
1331 package in Python to match specific motifs, which are indicated in the figure legends.
1332
1333 To search for the transcription factor binding sites, we used FIMO[61] to scan for motifs in
1334 HOCOMOCO v11 core motifs database[62].
1335
1336 **RNA secondary prediction and minimal free energy calculation**
1337 ViennaRNA package (version 2.5.1) was used to perform RNA secondary structure prediction[63].
1338 The RNAfold Python API “RNA” was used in the analysis. The folding temperature was set to
1339 37°C. The minimum free energy of the predicted structure was used.
1340
1341 **QUANTIFICATION AND STATISTICAL ANALYSIS**
1342
1343 Quantitative and statistical methods are described above and in figure legends according to
1344 their respective technologies and analytic approaches. Statistical analysis and visualization
1345 were mainly performed with Python (version 3.8.7). R (version 4.2.2) was used in differential
1346 gene expression analysis and Gene Ontology analysis.
1347
1348 Versions of key Python packages: numpy (1.23.5); pandas (1.5.2); scipy (1.9.3); matplotlib
1349 (3.6.2); seaborn (0.12.1); matplotlib-venn (0.11.9).
1350
1351 Versions of key R packages: DESeq2 (1.38.1); clusterProfiler (4.6.0); enrichplot (1.18.3);
1352 GOSemSim (2.24.0); org.Hs.eg.db (3.16.0).
1353
1354 All boxplots and violin plot summary statistics show the median and IQR of the underlying data.
1355 Statistical tests are described in the appropriate figure legends. Student’s t-test was applied for
1356 two sample non-paired comparisons. One-sided or two-sided testing was performed according

to figure legends. If possible, we omitted significance “stars” from figures; p-values (or equivalent) are instead reported.

DATA AND CODE AVAILABILITY

All sequencing data can be accessed from NCBI Gene Expression Omnibus: GSE188510 for ReCappable-seq; GSE233655 for CROWN-seq data.

Because of the size limit of supplemental tables, several large tables (e.g., the table for all mRNA m^6Am sites quantified in this study) were not directly included in the **Supplemental Tables**. These large supplemental tables have been uploaded to Zenodo: https://zenodo.org/records/12760731 (DOI: 10.5281/zenodo.12760731).

All original code has been deposited on GitHub:

- ReCappable-seq analysis: https://github.com/jhfoxliu/ReCappable-seq
- GLORI analysis: https://github.com/jhfoxliu/GLORI_pipeline
- CROWN-seq analysis: https://github.com/jhfoxliu/CROWN-seq

Any additional information required to reanalyze the data reported in this paper is available from the lead contact upon request.

MATERIALS AVAILABILITY

This study did not generate new unique reagents.

REFERENCES

1. Wang, J., Alvin Chew, B.L., Lai, Y., Dong, H., Xu, L., Balamkundu, S., Cai, W.M., Cui, L., Liu, C.F., Fu, X.Y., Lin, Z., Shi, P.Y., Lu, T.K., Luo, D., Jaffrey, S.R., and Dedon, P.C. (2019). Quantifying the RNA cap epitranscriptome reveals novel caps in cellular and viral RNA. Nucleic Acids Res *47*, e130. 10.1093/nar/gkz751.

2. Galloway, A., Atrih, A., Grzela, R., Darzynkiewicz, E., Ferguson, M.A.J., and Cowling, V.H. (2020). CAP-MAP: cap analysis protocol with minimal analyte processing, a rapid and sensitive approach to analysing mRNA cap structures. Open Biol *10*, 190306. 10.1098/rsob.190306.

3. Bélanger, F., Stepinski, J., Darzynkiewicz, E., and Pelletier, J. (2010). Characterization of hMTr1, a human Cap1 2′-O-ribose methyltransferase. Journal of Biological Chemistry *285*, 33037-33044.

4. Akichika, S., Hirano, S., Shichino, Y., Suzuki, T., Nishimasu, H., Ishitani, R., Sugita, A., Hirose, Y., Iwasaki, S., Nureki, O., and Suzuki, T. (2019). Cap-specific terminal N (6)-methylation of RNA by an RNA polymerase II-associated methyltransferase. Science *363*, eaav0080. 10.1126/science.aav0080.

1399 5. Wang, L., Wu, L., Zhu, Z., Zhang, Q., Li, W., Gonzalez, G.M., Wang, Y., and Rana, T.M.
1400 (2023). Role of PCIF1-mediated 5′-cap N6-methyladeonsine mRNA methylation in
1401 colorectal cancer and anti-PD-1 immunotherapy. The EMBO Journal *42*, e111673.

1402 6. Zhang, Q., Kang, Y., Wang, S., Gonzalez, G.M., Li, W., Hui, H., Wang, Y., and Rana,
1403 T.M. (2021). HIV reprograms host m(6)Am RNA methylome by viral Vpr protein-
1404 mediated degradation of PCIF1. Nat Commun *12*, 5543. 10.1038/s41467-021-25683-4.

1405 7. Wang, L., Wang, S., Wu, L., Li, W., Bray, W., Clark, A.E., Gonzalez, G.M., Wang, Y.,
1406 Carlin, A.F., and Rana, T.M. (2023). PCIF1-mediated deposition of 5'-cap N(6),2'-O-
1407 dimethyladenosine in ACE2 and TMPRSS2 mRNA regulates susceptibility to SARS-
1408 CoV-2 infection. Proc Natl Acad Sci U S A *120*, e2210361120.
1409 10.1073/pnas.2210361120.

1410 8. Tartell, M.A., Boulias, K., Hoffmann, G.B., Bloyet, L.M., Greer, E.L., and Whelan, S.P.J.
1411 (2021). Methylation of viral mRNA cap structures by PCIF1 attenuates the antiviral
1412 activity of interferon-beta. Proc Natl Acad Sci U S A *118*, e2025769118.
1413 10.1073/pnas.2025769118.

1414 9. Wei, C.M., Gershowitz, A., and Moss, B. (1975). Methylated nucleotides block 5'
1415 terminus of HeLa cell messenger RNA. Cell *4*, 379-386. 10.1016/0092-8674(75)90158-
1416 0.

1417 10. Mauer, J., Sindelar, M., Despic, V., Guez, T., Hawley, B.R., Vasseur, J.-J., Rentmeister,
1418 A., Gross, S.S., Pellizzoni, L., and Debart, F. (2019). FTO controls reversible m6Am
1419 RNA methylation during snRNA biogenesis. Nature chemical biology *15*, 340-347.

1420 11. Sun, H., Li, K., Zhang, X., Liu, J.e., Zhang, M., Meng, H., and Yi, C. (2021). m6Am-seq
1421 reveals the dynamic m6Am methylation in the human transcriptome. Nature
1422 Communications *12*, 4778.

1423 12. Koh, C.W., Goh, Y.T., and Goh, W.S. (2019). Atlas of quantitative single-base-resolution
1424 N 6-methyl-adenine methylomes. Nature communications *10*, 5636.

1425 13. Sendinc, E., Valle-Garcia, D., Dhall, A., Chen, H., Henriques, T., Navarrete-Perea, J.,
1426 Sheng, W., Gygi, S.P., Adelman, K., and Shi, Y. (2019). PCIF1 Catalyzes m6Am mRNA
1427 Methylation to Regulate Gene Expression. Mol Cell *75*, 620-630 e629.
1428 10.1016/j.molcel.2019.05.030.

1429 14. Boulias, K., Toczydlowska-Socha, D., Hawley, B.R., Liberman, N., Takashima, K.,
1430 Zaccara, S., Guez, T., Vasseur, J.J., Debart, F., Aravind, L., Jaffrey, S.R., and Greer,
1431 E.L. (2019). Identification of the m(6)Am Methyltransferase PCIF1 Reveals the Location
1432 and Functions of m(6)Am in the Transcriptome. Mol Cell *75*, 631-643 e638.
1433 10.1016/j.molcel.2019.06.006.

1434 15. Mauer, J., Luo, X., Blanjoie, A., Jiao, X., Grozhik, A.V., Patil, D.P., Linder, B., Pickering,
1435 B.F., Vasseur, J.-J., and Chen, Q. (2017). Reversible methylation of m6Am in the 5′ cap
1436 controls mRNA stability. Nature *541*, 371-375.

1437 16. Noguchi, S., Arakawa, T., Fukuda, S., Furuno, M., Hasegawa, A., Hori, F., Ishikawa-
1438 Kato, S., Kaida, K., Kaiho, A., and Kanamori-Katayama, M. (2017). FANTOM5 CAGE
1439 profiles of human and mouse samples. Scientific data *4*, 1-10.

1440 17. Dönmez, G., Hartmuth, K., and Lührmann, R. (2004). Modified nucleotides at the 5′ end
1441 of human U2 snRNA are required for spliceosomal E-complex formation. Rna *10*, 1925-
1442 1933.

1443 18. Yan, B., Tzertzinis, G., Schildkraut, I., and Ettwiller, L. (2022). Comprehensive
1444 determination of transcription start sites derived from all RNA polymerases using
1445 ReCappable-seq. Genome Research *32*, 162-174.

1446 19. Yamashita, R., Sathira, N.P., Kanai, A., Tanimoto, K., Arauchi, T., Tanaka, Y.,
1447 Hashimoto, S.-i., Sugano, S., Nakai, K., and Suzuki, Y. (2011). Genome-wide
1448 characterization of transcriptional start sites in humans by integrative transcriptome
1449 analysis. Genome research *21*, 775-789.

1450 20. Liu, C., Sun, H., Yi, Y., Shen, W., Li, K., Xiao, Y., Li, F., Li, Y., Hou, Y., Lu, B., Liu, W.,
1451 Meng, H., Peng, J., Yi, C., and Wang, J. (2023). Absolute quantification of single-base
1452 m(6)A methylation in the mammalian transcriptome using GLORI. Nat Biotechnol *41*,
1453 355-366. 10.1038/s41587-022-01487-9.

1454 21. Mahdavi-Amiri, Y., Chung, K.C.K., and Hili, R. (2021). Single-nucleotide resolution of N
1455 6-adenine methylation sites in DNA and RNA by nitrite sequencing. Chemical science
1456 *12*, 606-612.

1457 22. Werner, S., Galliot, A., Pichot, F., Kemmer, T., Marchand, V., Sednev, M.V., Lence, T.,
1458 Roignant, J.-Y., König, J., and Höbartner, C. (2021). NOseq: amplicon sequencing
1459 evaluation method for RNA m6A sites after chemical deamination. Nucleic Acids
1460 Research *49*, e23-e23.

1461 23. HAVANA gene annotation guildelines. https://www.sanger.ac.uk/project/manual-
1462 annotation/.

1463 24. Li, K., Chen, J., Zhang, C., Cheng, M., Chen, S., Song, W., Yang, C., Ling, R., Chen, Z.,
1464 and Wang, X. (2023). The CTBP2-PCIF1 complex regulates m 6 Am modification of
1465 mRNA in head and neck squamous cell carcinoma. The Journal of Clinical Investigation
1466 *133*.

1467 25. Djebali, S., Davis, C.A., Merkel, A., Dobin, A., Lassmann, T., Mortazavi, A., Tanzer, A.,
1468 Lagarde, J., Lin, W., and Schlesinger, F. (2012). Landscape of transcription in human
1469 cells. Nature *489*, 101-108.

1470 26. Marzluff, W.F., and Koreski, K.P. (2017). Birth and Death of Histone mRNAs. Trends
1471 Genet *33*, 745-759. 10.1016/j.tig.2017.07.014.

1472 27. Fan, H., Sakuraba, K., Komuro, A., Kato, S., Harada, F., and Hirose, Y. (2003). PCIF1, a
1473 novel human WW domain-containing protein, interacts with the phosphorylated RNA
1474 polymerase II. Biochemical and biophysical research communications *301*, 378-385.

1475 28. Sugita, A., Kuruma, S., Yanagisawa, N., Ishiguro, H., Kano, R., Ohkuma, Y., and Hirose,
1476 Y. (2021). The cap-specific m6A methyltransferase, PCIF1/CAPAM, is dynamically
1477 recruited to the gene promoter in a transcription-dependent manner. The journal of
1478 biochemistry *170*, 203-213.

1479 29. Haberle, V., and Stark, A. (2018). Eukaryotic core promoters and the functional basis of
1480 transcription initiation. Nature reviews Molecular cell biology *19*, 621-637.

1481 30. Zhang, Z., Chen, L.-Q., Zhao, Y.-L., Yang, C.-G., Roundtree, I.A., Zhang, Z., Ren, J.,
1482 Xie, W., He, C., and Luo, G.-Z. (2019). Single-base mapping of m6A by an antibody-
1483 independent method. Science advances *5*, eaax0250.

1484 31. Kiss, T. (2004). Biogenesis of small nuclear RNPs. Journal of cell science *117*, 5949-
1485 5951.

1486 32. Huang, Z.-h., Du, Y.-p., Wen, J.-t., Lu, B.-f., and Zhao, Y. (2022). snoRNAs: functions
1487 and mechanisms in biological processes, and roles in tumor pathophysiology. Cell Death
1488 Discovery *8*, 259.

1489 33. Huang, T., Chen, W., Liu, J., Gu, N., and Zhang, R. (2019). Genome-wide identification
1490 of mRNA 5-methylcytosine in mammals. Nature structural & molecular biology *26*, 380-
1491 388.

1492 34. Zhang, Z., Chen, T., Chen, H.-X., Xie, Y.-Y., Chen, L.-Q., Zhao, Y.-L., Liu, B.-D., Jin, L.,
1493 Zhang, W., and Liu, C. (2021). Systematic calibration of epitranscriptomic maps using a
1494 synthetic modification-free RNA library. Nature Methods *18*, 1213-1222.

1495 35. Knutson, S.D., Sanford, A.A., Swenson, C.S., Korn, M.M., Manuel, B.A., and Heemstra,
1496 J.M. (2020). Thermoreversible control of nucleic acid structure and function with glyoxal
1497 caging. Journal of the American Chemical Society *142*, 17766-17781.

1498 36. Rong, M., He, B., McAllister, W.T., and Durbin, R.K. (1998). Promoter specificity
1499 determinants of T7 RNA polymerase. Proceedings of the National Academy of Sciences
1500 *95*, 515-519.

1501 37. Dousis, A., Ravichandran, K., Hobert, E.M., Moore, M.J., and Rabideau, A.E. (2023). An
1502 engineered T7 RNA polymerase that produces mRNA free of immunostimulatory
1503 byproducts. Nature biotechnology *41*, 560-568.

1504 38. Legrand, C., Tuorto, F., Hartmann, M., Liebers, R., Jacob, D., Helm, M., and Lyko, F.
1505 (2017). Statistically robust methylation calling for whole-transcriptome bisulfite
1506 sequencing reveals distinct methylation patterns for mouse RNAs. Genome research *27*,
1507 1589-1596.

1508 39. An, H., Hong, Y., Goh, Y.T., Koh, C.W., Kanwal, S., Zhang, Y., Lu, Z., Yap, P.M., Neo,
1509 S.P., and Wong, C.-M. (2024). m6Am sequesters PCF11 to suppress premature
1510 termination and drive neuroblastoma differentiation. Molecular Cell *84*, 4142-4157.
1511 e4114.

1512 40. Wang, X., Lu, Z., Gomez, A., Hon, G.C., Yue, Y., Han, D., Fu, Y., Parisien, M., Dai, Q.,
1513 and Jia, G. (2014). N 6-methyladenosine-dependent regulation of messenger RNA
1514 stability. Nature *505*, 117-120.

1515 41. Patil, D.P., Chen, C.-K., Pickering, B.F., Chow, A., Jackson, C., Guttman, M., and
1516 Jaffrey, S.R. (2016). m6A RNA methylation promotes XIST-mediated transcriptional
1517 repression. Nature *537*, 369-373.

1518 42. Mimoso, C.A., and Adelman, K. (2023). U1 snRNP increases RNA Pol II elongation rate
1519 to enable synthesis of long genes. Molecular cell *83*, 1264-1279. e1210.

1520 43. Mauer, J., and Jaffrey, S.R. (2018). FTO, m6Am, and the hypothesis of reversible
1521 epitranscriptomic mRNA modifications. FEBS letters *592*, 2012-2022.

1522 44. Linder, B., Grozhik, A.V., Olarerin-George, A.O., Meydan, C., Mason, C.E., and Jaffrey,
1523 S.R. (2015). Single-nucleotide-resolution mapping of m6A and m6Am throughout the
1524 transcriptome. Nature methods *12*, 767-772.

1525 45. Love, M.I., Huber, W., and Anders, S. (2014). Moderated estimation of fold change and
1526 dispersion for RNA-seq data with DESeq2. Genome biology *15*, 1-21.

1527 46. Vigneault, F., Ter-Ovanesyan, D., Alon, S., Eminaga, S., C. Christodoulou, D., Seidman,
1528 J., Eisenberg, E., and M. Church, G. (2012). High-throughput multiplex sequencing of
1529 miRNA. Current Protocols in Human Genetics *73*, 11.12. 11-11.12. 10.

1530 47. Huang, T., Chen, W., Liu, J., Gu, N., and Zhang, R. (2019). Genome-wide identification
1531 of mRNA 5-methylcytosine in mammals. Nat Struct Mol Biol *26*, 380-388.
1532 10.1038/s41594-019-0218-x.

1533 48. Martin, M. (2011). Cutadapt removes adapter sequences from high-throughput
1534 sequencing reads. EMBnet. journal *17*, 10-12.

1535 49. Kim, D., Paggi, J.M., Park, C., Bennett, C., and Salzberg, S.L. (2019). Graph-based
1536 genome alignment and genotyping with HISAT2 and HISAT-genotype. Nat Biotechnol
1537 *37*, 907-915. 10.1038/s41587-019-0201-4.

1538 50. Li, H., Handsaker, B., Wysoker, A., Fennell, T., Ruan, J., Homer, N., Marth, G.,
1539 Abecasis, G., Durbin, R., and Genome Project Data Processing, S. (2009). The
1540 Sequence Alignment/Map format and SAMtools. Bioinformatics *25*, 2078-2079.
1541 10.1093/bioinformatics/btp352.

1542 51. Smith, T., Heger, A., and Sudbery, I. (2017). UMI-tools: modeling sequencing errors in
1543 Unique Molecular Identifiers to improve quantification accuracy. Genome Res *27*, 491-
1544 499. 10.1101/gr.209601.116.

1545 52. Langmead, B., and Salzberg, S.L. (2012). Fast gapped-read alignment with Bowtie 2.
1546 Nat Methods *9*, 357-359. 10.1038/nmeth.1923.

1547 53. Quinlan, A.R., and Hall, I.M. (2010). BEDTools: a flexible suite of utilities for comparing
1548 genomic features. Bioinformatics *26*, 841-842. 10.1093/bioinformatics/btq033.

1549 54. Risso, D., Ngai, J., Speed, T.P., and Dudoit, S. (2014). Normalization of RNA-seq data
1550 using factor analysis of control genes or samples. Nature biotechnology *32*, 896-902.

1551 55. Mair, S., Erharter, K., Renard, E., Brillet, K., Brunner, M., Lusser, A., Kreutz, C., Ennifar,
1552 E., and Micura, R. (2022). Towards a comprehensive understanding of RNA
1553 deamination: synthesis and properties of xanthosine-modified RNA. Nucleic Acids
1554 Research *50*, 6038-6051.

1555 56. Camacho, C., Coulouris, G., Avagyan, V., Ma, N., Papadopoulos, J., Bealer, K., and
1556 Madden, T.L. (2009). BLAST+: architecture and applications. BMC bioinformatics *10*, 1-
1557 9.

1558 57. Manske, F., Ogoniak, L., Jürgens, L., Grundmann, N., Makałowski, W., and Wethmar, K.
1559 (2023). The new uORFdb: integrating literature, sequence, and variation data in a
1560 central hub for uORF research. Nucleic Acids Research *51*, D328-D336.

1561 58. Yang, T.-H., Wang, C.-Y., Tsai, H.-C., and Liu, C.-T. (2021). Human IRES Atlas: an
1562 integrative platform for studying IRES-driven translational regulation in humans.
1563 Database *2021*, baab025.

1564 59. Yu, G., Wang, L.-G., Han, Y., and He, Q.-Y. (2012). clusterProfiler: an R package for
1565 comparing biological themes among gene clusters. Omics: a journal of integrative
1566 biology *16*, 284-287.

1567 60. Yu, G., Li, F., Qin, Y., Bo, X., Wu, Y., and Wang, S. (2010). GOSemSim: an R package
1568 for measuring semantic similarity among GO terms and gene products. Bioinformatics
1569 *26*, 976-978.

1570 61. Grant, C.E., Bailey, T.L., and Noble, W.S. (2011). FIMO: scanning for occurrences of a
1571 given motif. Bioinformatics *27*, 1017-1018.

1572 62. Kulakovskiy, I.V., Vorontsov, I.E., Yevshin, I.S., Sharipov, R.N., Fedorova, A.D.,
1573 Rumynskiy, E.I., Medvedeva, Y.A., Magana-Mora, A., Bajic, V.B., and Papatsenko, D.A.
1574 (2018). HOCOMOCO: towards a complete collection of transcription factor binding
1575 models for human and mouse via large-scale ChIP-Seq analysis. Nucleic acids research
1576 *46*, D252-D259.

1577 63. Lorenz, R., Bernhart, S.H., Höner zu Siederdissen, C., Tafer, H., Flamm, C., Stadler,
1578 P.F., and Hofacker, I.L. (2011). ViennaRNA Package 2.0. Algorithms for molecular
1579 biology *6*, 1-14.
1580
1581

Figure 1

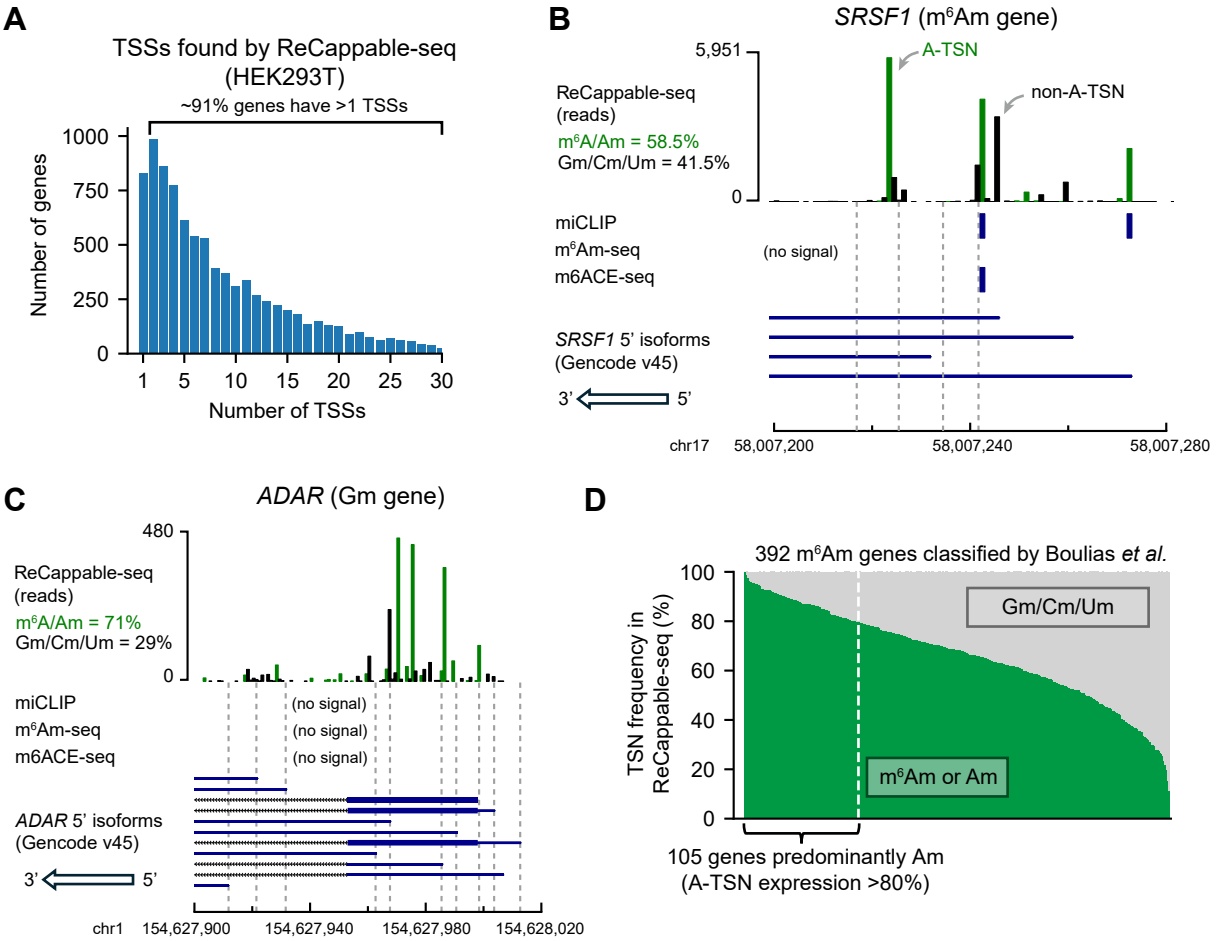
A
TSSs found by ReCappable-seq
(HEK293T)
~91% genes have >1 TSSs
Number of genes
1000
750
500
250
0
1
5
10
15
20
25
30
Number of TSSs
B
SRSF1 (m6Am gene)
5,951
A-TSN
non-A-TSN
ReCappable-seq
(reads)
m6A/Am = 58.5%
Gm/Cm/Um = 41.5%
0
miCLIP
m6Am-seq
m6ACE-seq
(no signal)
SRSF1 5' isoforms
(Gencode v45)
3'
5'
chr17
58,007,200
58,007,240
58,007,280
C
ADAR (Gm gene)
480
ReCappable-seq
(reads)
m6A/Am = 71%
Gm/Cm/Um = 29%
0
miCLIP
m6Am-seq
m6ACE-seq
(no signal)
(no signal)
(no signal)
ADAR 5' isoforms
(Gencode v45)
3'
5'
chr1
154,627,900
154,627,940
154,627,980
154,628,020
D
392 m6Am genes classified by Boulias et al.
TSN frequency in
ReCappable-seq (%)
100
80
60
40
20
0
Gm/Cm/Um
m6Am or Am
105 genes predominantly Am
(A-TSN expression >80%)

Figure 2

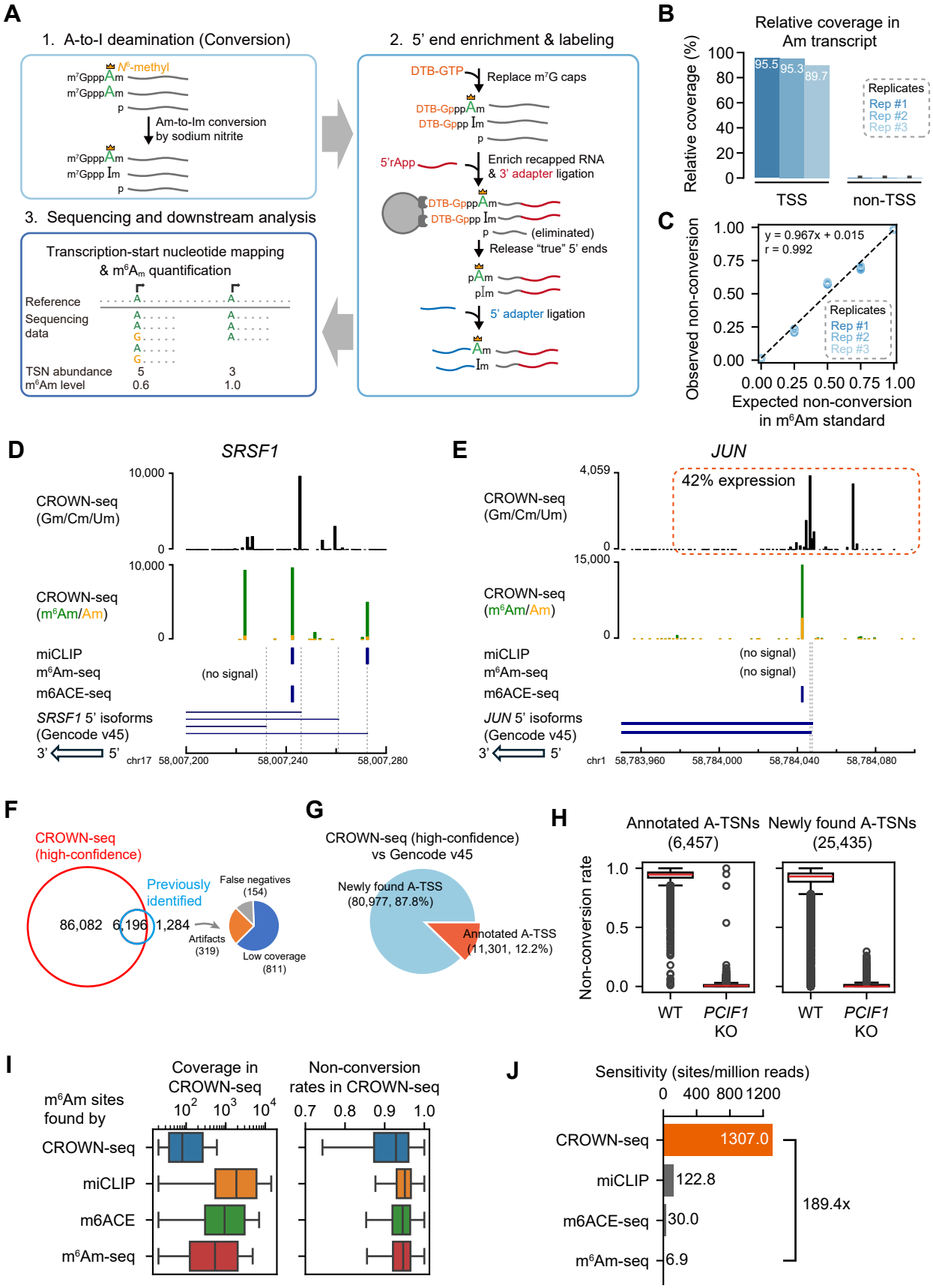
A
1. A-to-I deamination (Conversion)
N6-methyl
m7GpppAm
m7GpppAm
p
Am-to-Im conversion by sodium nitrite
m7GpppAm
m7Gppp Im
p
2. 5' end enrichment & labeling
DTB-GTP
Replace m7G caps
DTB-GpppAm
DTB-Gppp Im
p
5'rApp
Enrich recapped RNA & 3' adapter ligation
DTB-GpppAm
DTB-Gppp Im
p
(eliminated)
Release "true" 5' ends
pAm
pIm
5' adapter ligation
Am
Im
3. Sequencing and downstream analysis
Transcription-start nucleotide mapping & m6Am quantification
Reference
Sequencing data
TSN abundance 5 3
m6Am level 0.6 1.0
B
Relative coverage in Am transcript
Relative coverage (%)
95.5
95.3
89.7
Replicates
Rep #1
Rep #2
Rep #3
TSS
non-TSS
C
y = 0.967x + 0.015
r = 0.992
Observed non-conversion
Expected non-conversion in m6Am standard
D
SRSF1
CROWN-seq (Gm/Cm/Um)
CROWN-seq (m6Am/Am)
miCLIP
m6Am-seq
m6ACE-seq
(no signal)
SRSF1 5' isoforms (Gencode v45)
chr17 58,007,200 58,007,240 58,007,280
E
JUN
42% expression
CROWN-seq (Gm/Cm/Um)
CROWN-seq (m6Am/Am)
miCLIP
m6Am-seq
m6ACE-seq
(no signal)
JUN 5' isoforms (Gencode v45)
chr1 58,783,960 58,784,000 58,784,040 58,784,080
F
CROWN-seq (high-confidence)
Previously identified
86,082 6,196 1,284
False negatives (154)
Artifacts (319)
Low coverage (811)
G
CROWN-seq (high-confidence) vs Gencode v45
Newly found A-TSS (80,977, 87.8%)
Annotated A-TSS (11,301, 12.2%)
H
Annotated A-TSNs (6,457)
Newly found A-TSNs (25,435)
Non-conversion rate
WT
PCIF1 KO
I
m6Am sites found by
Coverage in CROWN-seq
Non-conversion rates in CROWN-seq
CROWN-seq
miCLIP
m6ACE
m6Am-seq
J
Sensitivity (sites/million reads)
CROWN-seq 1307.0
miCLIP 122.8
m6ACE-seq 30.0
m6Am-seq 6.9
189.4x

Figure 3

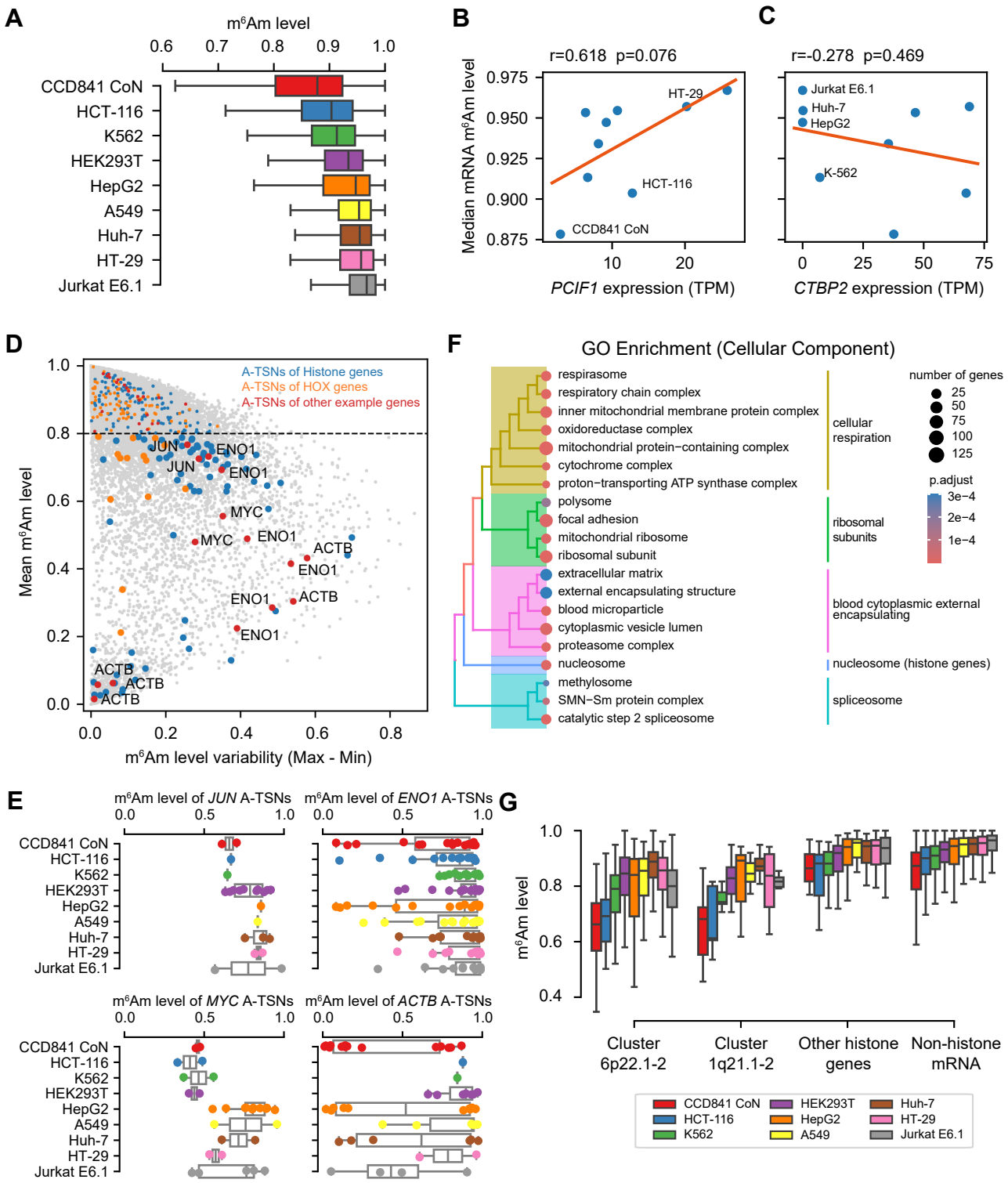
A
m6Am level
0.6 0.7 0.8 0.9 1.0
CCD841 CoN
HCT-116
K562
HEK293T
HepG2
A549
Huh-7
HT-29
Jurkat E6.1
B
r=0.618 p=0.076
Median mRNA m6Am level
0.975
0.950
0.925
0.900
0.875
HT-29
HCT-116
CCD841 CoN
10 20
PCIF1 expression (TPM)
C
r=-0.278 p=0.469
Jurkat E6.1
Huh-7
HepG2
K-562
0 25 50 75
CTBP2 expression (TPM)
D
A-TSNs of Histone genes
A-TSNs of HOX genes
A-TSNs of other example genes
Mean m6Am level
1.0
0.8
0.6
0.4
0.2
0.0
JUN
ENO1
MYC
ACTB
0.0 0.2 0.4 0.6 0.8
m6Am level variability (Max - Min)
F
GO Enrichment (Cellular Component)
respirasome
respiratory chain complex
inner mitochondrial membrane protein complex
oxidoreductase complex
mitochondrial protein−containing complex
cytochrome complex
proton−transporting ATP synthase complex
polysome
focal adhesion
mitochondrial ribosome
ribosomal subunit
extracellular matrix
external encapsulating structure
blood microparticle
cytoplasmic vesicle lumen
proteasome complex
nucleosome
methylosome
SMN−Sm protein complex
catalytic step 2 spliceosome
cellular respiration
ribosomal subunits
blood cytoplasmic external encapsulating
nucleosome (histone genes)
spliceosome
number of genes
25
50
75
100
125
p.adjust
3e−4
2e−4
1e−4
E
m6Am level of JUN A-TSNs
m6Am level of ENO1 A-TSNs
m6Am level of MYC A-TSNs
m6Am level of ACTB A-TSNs
0.0 0.5 1.0
CCD841 CoN
HCT-116
K562
HEK293T
HepG2
A549
Huh-7
HT-29
Jurkat E6.1
G
m6Am level
1.0
0.8
0.6
0.4
Cluster 6p22.1-2
Cluster 1q21.1-2
Other histone genes
Non-histone mRNA
CCD841 CoN
HCT-116
K562
HEK293T
HepG2
A549
Huh-7
HT-29
Jurkat E6.1

Figure 4

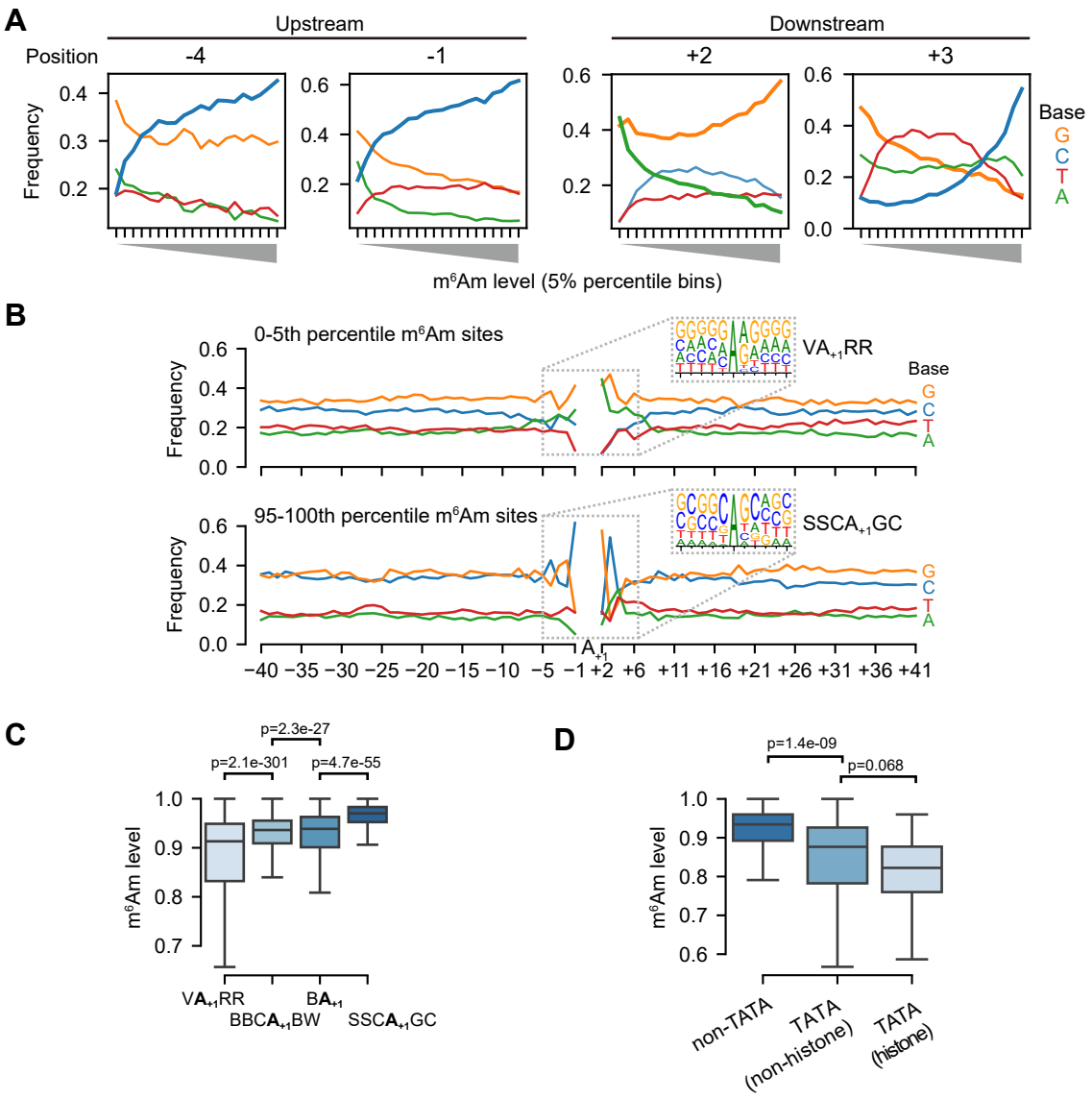
A
Upstream
Downstream
Position
-4
-1
+2
+3
Frequency
Base
G
C
T
A
m6Am level (5% percentile bins)
B
0-5th percentile m6Am sites
VA+1RR
95-100th percentile m6Am sites
SSCA+1GC
Frequency
A+1
−40 −35 −30 −25 −20 −15 −10 −5 −1 +2 +6 +11 +16 +21 +26 +31 +36 +41
C
p=2.3e-27
p=2.1e-301
p=4.7e-55
m6Am level
VA+1RR
BA+1
BBCA+1BW
SSCA+1GC
D
p=1.4e-09
p=0.068
m6Am level
non-TATA
TATA (non-histone)
TATA (histone)

Figure 5

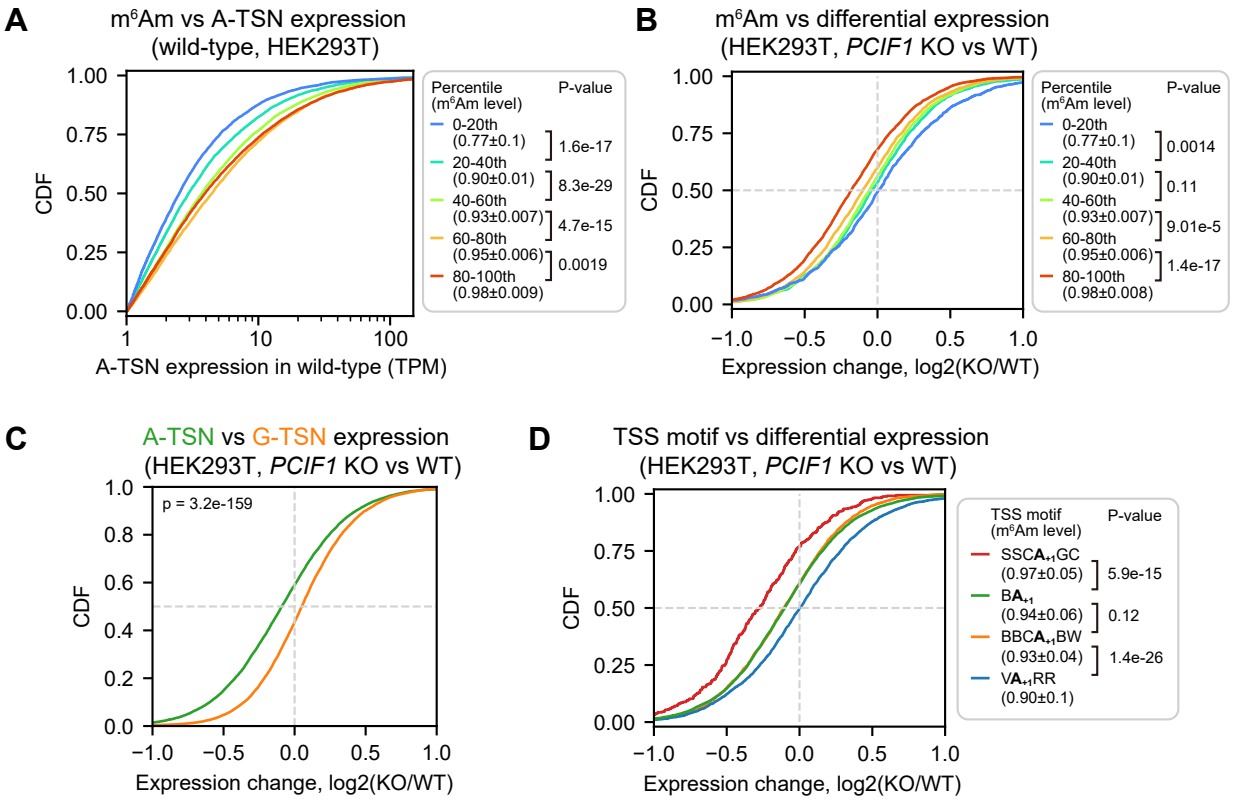
A
m6Am vs A-TSN expression
(wild-type, HEK293T)
CDF
A-TSN expression in wild-type (TPM)
Percentile (m6Am level)
P-value
0-20th (0.77±0.1)
20-40th (0.90±0.01)
40-60th (0.93±0.007)
60-80th (0.95±0.006)
80-100th (0.98±0.009)
1.6e-17
8.3e-29
4.7e-15
0.0019
B
m6Am vs differential expression
(HEK293T, PCIF1 KO vs WT)
CDF
Expression change, log2(KO/WT)
Percentile (m6Am level)
P-value
0-20th (0.77±0.1)
20-40th (0.90±0.01)
40-60th (0.93±0.007)
60-80th (0.95±0.006)
80-100th (0.98±0.008)
0.0014
0.11
9.01e-5
1.4e-17
C
A-TSN vs G-TSN expression
(HEK293T, PCIF1 KO vs WT)
p = 3.2e-159
CDF
Expression change, log2(KO/WT)
D
TSS motif vs differential expression
(HEK293T, PCIF1 KO vs WT)
CDF
Expression change, log2(KO/WT)
TSS motif (m6Am level)
P-value
SSCA+1GC (0.97±0.05)
BA+1 (0.94±0.06)
BBCA+1BW (0.93±0.04)
VA+1RR (0.90±0.1)
5.9e-15
0.12
1.4e-26

Figure 6

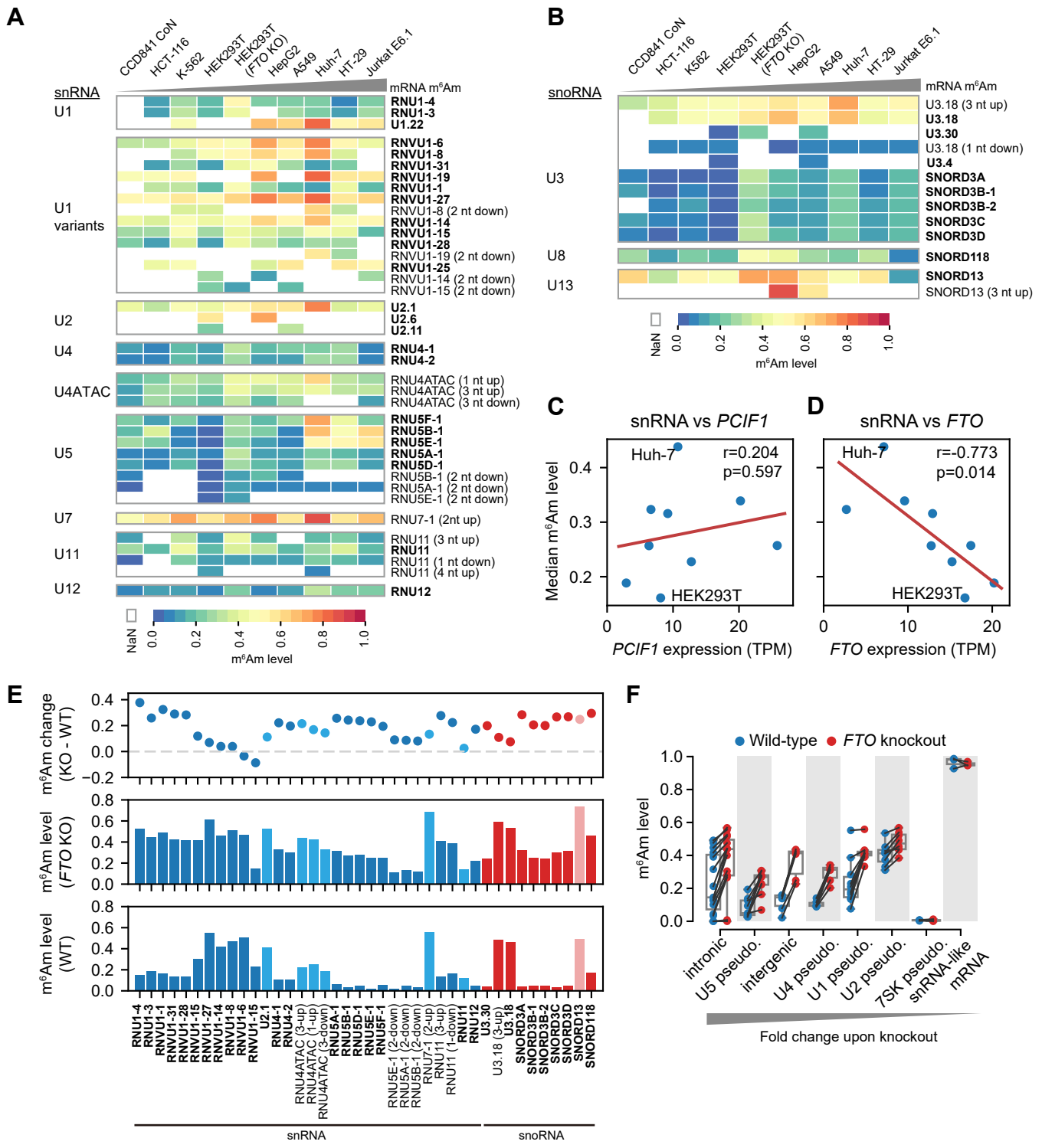
A
CCD841 CoN
HCT-116
K-562
HEK293T
HEK293T (FTO KO)
HepG2
A549
Huh-7
HT-29
Jurkat E6.1
mRNA m6Am
snRNA
U1
RNU1-4
RNU1-3
U1.22
U1 variants
RNVU1-6
RNVU1-8
RNVU1-31
RNVU1-19
RNVU1-1
RNVU1-27
RNVU1-8 (2 nt down)
RNVU1-14
RNVU1-15
RNVU1-28
RNVU1-19 (2 nt down)
RNVU1-25
RNVU1-14 (2 nt down)
RNVU1-15 (2 nt down)
U2
U2.1
U2.6
U2.11
U4
RNU4-1
RNU4-2
U4ATAC
RNU4ATAC (1 nt up)
RNU4ATAC (3 nt up)
RNU4ATAC (3 nt down)
U5
RNU5F-1
RNU5B-1
RNU5E-1
RNU5A-1
RNU5D-1
RNU5B-1 (2 nt down)
RNU5A-1 (2 nt down)
RNU5E-1 (2 nt down)
U7
RNU7-1 (2nt up)
U11
RNU11 (3 nt up)
RNU11
RNU11 (1 nt down)
RNU11 (4 nt up)
U12
RNU12
NaN
0.0
0.2
0.4
0.6
0.8
1.0
m6Am level
B
snoRNA
U3
U3.18 (3 nt up)
U3.18
U3.30
U3.18 (1 nt down)
U3.4
SNORD3A
SNORD3B-1
SNORD3B-2
SNORD3C
SNORD3D
U8
SNORD118
U13
SNORD13
SNORD13 (3 nt up)
C
snRNA vs PCIF1
Huh-7
r=0.204
p=0.597
HEK293T
Median m6Am level
PCIF1 expression (TPM)
D
snRNA vs FTO
Huh-7
r=-0.773
p=0.014
HEK293T
FTO expression (TPM)
E
m6Am change (KO - WT)
m6Am level (FTO KO)
m6Am level (WT)
snRNA
snoRNA
F
Wild-type
FTO knockout
m6Am level
intronic
U5 pseudo.
intergenic
U4 pseudo.
U1 pseudo.
U2 pseudo.
7SK pseudo.
snRNA-like
mRNA
Fold change upon knockout